SIAM J. APPL. MATH.
Vol. 72, No. 6, pp. 1869–1898

FAST AND ACCURATE COMPUTATION OF TIME-DOMAIN ACOUSTIC SCATTERING PROBLEMS WITH EXACT NONREFLECTING BOUNDARY CONDITIONS*

LI-LIAN WANG†, BO WANG‡, AND XIAODAN ZHAO†

Abstract. This paper is concerned with fast and accurate computation of exterior wave equations truncated via exact circular or spherical nonreflecting boundary conditions (NRBCs, known to be nonlocal in both time and space). We first derive analytic expressions for the underlying convolution kernels, which allow for a rapid and accurate evaluation of the convolution with $O(N_t)$ operations over N_t successive time steps. To handle the nonlocality in space, we introduce the notion of boundary perturbation, which enables us to handle general bounded scatters by solving a sequence of wave equations in a regular domain. We propose an efficient spectral-Galerkin solver with Newmark's time integration for the truncated wave equation in the regular domain. We also provide ample numerical results to show high-order accuracy of NRBCs and efficiency of the proposed scheme.

Key words. time-domain Dirichlet-to-Neumann map, nonreflecting boundary conditions, inverse Laplace transform, modified Bessel functions, convolution, spectral methods, Newmark's time integration

AMS subject classifications. 35J05, 35L05, 65R10, 65N35, 65E05, 65M70

DOI. 10.1137/110849146

1. Introduction.

Wave propagation and scattering problems in unbounded media arise from diverse application areas such as acoustics, aerodynamics, electromagnetics, antenna design, oceanography, and others (see, e.g., [20, 43, 14]). Various approaches have been proposed for their numerical simulation that include the boundary element methods (cf. [11]), infinite element methods (cf. [19]), perfectly matched layers (PML) (cf. [6]), nonreflecting boundary condition (NRBC) methods (cf. [28, 23]), and others (cf. [31, 49]). An essential ingredient for the latst approach is to truncate an unbounded domain to a bounded domain by imposing an exact or approximate nonreflecting (absorbing or transparent) boundary condition at the outer artificial boundary, where the NRBC is designed to prevent spurious wave reflection from the artificial boundary (cf. the review papers [20, 21] and the references therein). The frequency-domain approaches for, e.g., the time-harmonic Helmholtz problems have been intensively investigated, while the time-domain simulations, which are capable of capturing wide-band signals and modeling more general material inhomogeneities and nonlinearities (cf. [3, 13]), have been relatively less studied.

Although some types of NRBCs based on different principles have been proposed (see, e.g., [17, 5, 51, 44, 45, 22, 23, 21]), a longstanding issue of time-domain computation is the efficient treatment for NRBCs that can scale and integrate well with the solver for the underlying truncated problem (cf. [50, 24]). In practice, if an ac-

*Received by the editors September 26, 2011; accepted for publication (in revised form) July 31, 2012; published electronically December 6, 2012.
http://www.siam.org/journals/siap/72-6/84914.html
†Division of Mathematical Sciences, School of Physical and Mathematical Sciences, Nanyang Technological University, 637371, Singapore (lilian@ntu.edu.sg, zhao0122@e.ntu.edu.sg). The research of these authors was partially supported by Singapore AcRF Tier 1 grant RG58/08.
‡College of Mathematics and Computer Science, Hunan Normal University, Changsha, Hunan 410081, China, and Singapore-MIT Alliance, 4 Engineering Drive 3, National University of Singapore, Singapore 117576 (bowanghn@gmail.com).

curate NRBC is imposed, the artificial boundary could be placed as close as possible to the scatterer that can significantly reduce the computational cost. In this paper, we restrict our attention to the exact circular/spherical NRBC. One major difficulty lies in that such an NRBC is *global* in space and time in nature, as it involves the Fourier/spherical harmonic expressions in space, and history dependence in time induced by a convolution. The convolution kernel, termed a *nonreflecting boundary kernel* (NRBK) in [2], is the inverse Laplace transform of an expression that includes the logarithmic derivative of a modified Bessel function. The rapid computation of the NRBK and the involved convolution is of independent interest. Alpert, Greengard, and Hagstrom [2] proposed a rational approximation of the logarithmic derivative with a least squares implementation, which allows for a reduction of the use of poles from $O(\nu)$ to $O(\log\nu \log\frac{1}{\varepsilon})$ (where $\nu \gg 1$ is the order of the modified Bessel function and ε is a given tolerance) and a recursive convolution. Jiang and Greengard [26, 27] further considered some interesting applications to Schrödinger equations in one and two dimensions. Li [29] introduced a more accurate low-order approximation of the three-dimensional NRBK at a slightly expensive cost, where the observation that the Laplace transform of the three-dimensional NRBK is exactly a rational function lies at the heart of this algorithm. However, in many cases, the expressions are *not* rational functions. For instance, the two-dimensional NRBK also contains the contributions from the branch-cut along the negative real axis (see Theorem 2.2 below). Lubich and Schädle [30] developed some fast algorithm for the temporal convolution with $O(N_t \log N_t)$ operations (over N_t successive time steps) arising from NRBCs with nonrational expressions for other equations (e.g., Schrödinger equations and damped wave equations).

In this paper, we derive an analytic formula for the NRBK based on a direct inversion of the Laplace transform (see Theorem 2.2 below). In fact, Sofronov [45] presented some formulas of a similar type by working on much more complicated expressions of the kernel in terms of Tricomi's confluent hypergeometric functions. We show that with these formulas, we can evaluate the temporal convolution recursively and rapidly with $O(N_t)$ operations and almost without extra memory for the history dependence as in [2]. Moreover, the analytic expression provides a useful apparatus for the stability and convergence analysis. It is worthwhile to remark that Chen [9] reformulated the two-dimensional wave problem into a first-order system in time and showed the well-posedness of the truncated problem with an alternative formulation of the NRBC.

The nonlocality of the NRBC in space can be efficiently handled by Fourier/spherical harmonic expansions when the scatterer is a disk or a ball. Recently, a systematic approach, based on the boundary perturbation technique (also called the *transformed field expansion* (TFE) method (cf. [34])), has been developed in [35, 18, 36] for time-harmonic Helmholtz equations in exterior domains with general bounded obstacles, under which the whole algorithm boils down to solving a sequence of Helmholtz equations in a regular domain. In this paper, we highlight that this notion can be extended to time-domain computation, though it has not been investigated before as far as we know.

In this paper, we propose an efficient spectral-Galerkin method with Newmark's time integration for the truncated wave equations in an annulus or a spherical shell. We provide a practical approach to significantly reduce the computational cost for computing the NRBC via the analytic formulas advocated in this paper.

The rest of the paper is organized as follows. In section 2, we present the formulation of NRBCs and derive the analytic formulas for NRBKs. In section 3, we present some properties of NRBKs and analyze the well-posedness of the truncated

wave equation. In section 4, we outline the notion of the TFE method and propose an efficient spectral-Galerkin and Newmark's time integration scheme for the truncated problem in regular domains. We provide ample numerical results to show the accuracy and efficiency of the proposed approach in section 5.

2. Evaluation of nonreflecting boundary kernels. In this paper, we consider the time-domain acoustic scattering problem with sound-soft boundary conditions on the bounded obstacle:

$$\partial_t^2 U = c^2 \Delta U + F \quad \text{in } \Omega_\infty := \mathbb{R}^d \setminus \bar{D}, \ \ t > 0, \ \ d = 2, 3; \tag{2.1}$$

$$U = U_0, \quad \partial_t U = U_1 \quad \text{in } \Omega_\infty, \ \ t = 0; \tag{2.2}$$

$$U = G \quad \text{on } \Gamma_D, \ \ t > 0; \quad \partial_t U + c\partial_{\boldsymbol{n}} U = o(|\boldsymbol{x}|^{(1-d)/2}), \ \ |\boldsymbol{x}| \to \infty, \ \ t > 0, \tag{2.3}$$

where D is a bounded obstacle (scatterer) with Lipschitz boundary Γ_D, $c > 0$ is the wave speed, and $\boldsymbol{n} = \boldsymbol{x}/|\boldsymbol{x}|$. Assume that the data F, U_0, and U_1 are compactly supported in a two-dimensional disk or a three-dimensional ball B of radius b, which contains the obstacle D.

A common approach is to reduce this exterior problem to the problem in a bounded domain by imposing an exact or approximate NRBC at the artificial boundary $\Gamma_b := \partial B$. In what follows, we are concerned with the wave equation truncated by the exact circular/spherical NRBC:

$$\partial_t^2 U = c^2 \Delta U + F \quad \text{in } \Omega := B \setminus \bar{D}, \ \ t > 0, \ \ d = 2, 3; \tag{2.4}$$

$$U = U_0, \quad \partial_t U = U_1 \quad \text{in } \Omega, \ \ t = 0; \quad U = G \quad \text{on } \Gamma_D, \ \ t > 0; \tag{2.5}$$

$$\partial_r U = T_d(U) \quad \text{at } r = b, \ \ t > 0, \tag{2.6}$$

where $T_d(U)$ is the so-called time-domain Dirichlet-to-Neumann (DtN) map, to be specified below.

2.1. Formulation of $T_d(U)$. Here, we just present the expression of $T_d(U)$ in (2.6), and refer to, e.g., [23, 3] (and the original references therein) for the detailed derivation. It is known that the problem (2.1)–(2.3), exterior to $D = B$ with $F = U_0 = U_1 \equiv 0$ and $G = U|_{r=b}$ (i.e., the Dirichlet data taken from the interior problem (2.4)–(2.6)), can be solved analytically by using Laplace transform in time and separation of variables in space in polar coordinates (r, ϕ)/spherical coordinates (r, θ, ϕ). By imposing the continuity of the partial derivative with respect to r across the artificial boundary $r = b$, we obtain the boundary condition (2.6) with

$$T_d(U) = \begin{cases} \left(-\dfrac{1}{c}\dfrac{\partial U}{\partial t} - \dfrac{U}{2r} \right)\Big|_{r=b} + \displaystyle\sum_{|n|=0}^{\infty} \sigma_n(t) * \widehat{U}_n(b,t) e^{\mathrm{i}n\phi}, & d = 2, \\ \left(-\dfrac{1}{c}\dfrac{\partial U}{\partial t} - \dfrac{U}{r} \right)\Big|_{r=b} + \displaystyle\sum_{n=0}^{\infty} \sum_{|m|=0}^{n} \sigma_{n+1/2}(t) * \widehat{U}_{nm}(b,t) Y_n^m(\theta,\phi), & d = 3, \end{cases} \tag{2.7}$$

where

$$\sigma_\nu(t) := \mathcal{L}^{-1}\left[\frac{s}{c} + \frac{1}{2b} + \frac{s}{c}\frac{K_\nu'(sb/c)}{K_\nu(sb/c)} \right], \quad \nu = n, \ n + \frac{1}{2}. \tag{2.8}$$

Here, K_ν is the modified Bessel function of the second kind of order ν (see, e.g., [1, 52]), and $\mathcal{L}^{-1}[h(s)]$ is the inverse Laplace transform of a Laplace transformable

function $H(t)$:

$$h(s)=\mathcal{L}[H(t)](s)=\int_0^\infty H(t)e^{-st}\,dt,\quad s\in\mathbb{C},\ \ \mathrm{Re}(s)>0.$$

In (2.7), $\{Y_n^m\}$ are the spherical harmonics, which are orthonormal as defined in [32], and $\{\widehat{U}_n\}/\{\widehat{U}_{nm}\}$ are the Fourier/spherical harmonic expansion coefficients of $U|_{r=b}$. Recall that the convolution in (2.7) is defined as usual: $(f*g)(t)=\int_0^t f(t-\tau)g(\tau)d\tau$.

In the forthcoming analysis (see section 3), we find it is more convenient to use an alternative express of $T_d(U)$, where the temporal convolution is expressed in terms of expansion coefficients of $\partial_t U|_{r=b}$. More precisely, we define

$$\omega_\nu(t):=\omega_\nu(t;d):=-\frac{(d-1)c}{2b}+c\int_0^t\sigma_\nu(\tau)d\tau \tag{2.9}$$

and note that $\omega_\nu'(t)=c\sigma_\nu(t)$. Then, we find from (2.7) and integration by parts that

$$T_d(U)=-\frac{1}{c}\frac{\partial U}{\partial t}\Big|_{r=b}+\frac{1}{c}\begin{cases}\displaystyle\sum_{|n|=0}^{\infty}\omega_n(t)*\partial_t\widehat{U}_n(b,t)e^{\mathrm{i}n\phi}, & d=2,\\ \displaystyle\sum_{n=0}^{\infty}\sum_{|m|=0}^{n}\omega_{n+1/2}(t)*\partial_t\widehat{U}_{nm}(b,t)Y_n^m(\theta,\phi), & d=3,\end{cases} \tag{2.10}$$

where for $d=2,3$,

$$\omega_\nu(t)=\mathcal{L}^{-1}\left[1-\frac{(d-2)c}{2bs}+\frac{K_\nu'(sb/c)}{K_\nu(sb/c)}\right](t),\quad \nu=n,\ n+\frac{1}{2}. \tag{2.11}$$

Hereafter, we term σ_ν and ω_ν the nonreflecting boundary kernels (NRBKs). Since $K_{-n}(z)=K_n(z)$ (see Formula 9.6.6 in [1]), it suffices to consider ω_n and σ_n with $n\geq 0$ for $d=2$.

REMARK 2.1. *In the expressions of σ_ν and ω_ν, some terms are added, e.g., s/c and $1/(2b)$ in* (2.8)*, for the purpose of removing the singular part from the ratio K_ν'/K_ν. Indeed, recall the asymptotic formula for fixed $\nu\geq 0$ and large $|z|$ (see Formula* 9.7.2 *of* [1]):

$$K_\nu(z)\sim\sqrt{\frac{\pi}{2z}}e^{-z}\left\{1+\frac{4\nu^2-1}{8z}+O(z^{-2})\right\} \tag{2.12}$$

for $|\arg z|<3\pi/2$ (with a cut along the negative real axis), and the recurrence relation

$$zK_\nu'(z)=\nu K_\nu(z)-zK_{\nu+1}(z). \tag{2.13}$$

One verifies

$$\frac{K_\nu'(z)}{K_\nu(z)}\sim -1-\frac{1}{2z}+O(z^{-2}). \tag{2.14}$$

We see that NRBCs are global in both time and space. To solve the truncated problem (2.4)–(2.6) efficiently, we need to (i) invert the Laplace transform to compute NRBKs, (ii) deal with temporal convolutions efficiently, and (iii) handle the nonlocality of the NRBC in space effectively. The rest of the paper will address these issues.

2.2. Evaluation of the NRBKs. Our starting point is to invert the Laplace transform via evaluating the Bromwich's contour integral:

(2.15)
$$\sigma_\nu(t) = \frac{1}{2\pi \mathrm{i}} \int_{\gamma-\infty \mathrm{i}}^{\gamma+\infty \mathrm{i}} \left(\frac{s}{c} + \frac{1}{2b} + \frac{s}{c} \frac{K_\nu'(sb/c)}{K_\nu(sb/c)} \right) e^{ts} ds = \frac{c}{2b^2 \pi \mathrm{i}} \int_{\gamma-\infty \mathrm{i}}^{\gamma+\infty \mathrm{i}} F_\nu(z) e^{czt/b} dz$$

for $\nu = n, n+1/2$ with $n \geq 0$, where

(2.16)
$$F_\nu(z) = z + \frac{1}{2} + z \frac{K_\nu'(z)}{K_\nu(z)},$$

and γ is the Laplace convergence abscissa, which is a generic constant greater than the real part of any singularity of $F_\nu(z)$.

In order to use the residue theorem to evaluate (2.15), it is essential to understand the behavior of the poles of $F_\nu(z)$, i.e., the zeros of $K_\nu(z)$.

LEMMA 2.1. *Let $\nu \geq 0$ be a real number.*

(i) *If z is a zero of $K_\nu(z)$, then its complex conjugate $\bar{z}$ is also a zero. Moreover, all complex conjugate pairs of zeros lie in the second and third quadrants with* $\mathrm{Re}(z) < 0$.

(ii) *The total number of zeros of $K_\nu(z)$ is the even integer nearest to $\nu - 1/2$ if $\nu - 1/2$ is not an integer, or exactly $\nu - 1/2$ if $\nu - 1/2$ is an integer.*

(iii) *All zeros of $K_n(z)$ and $K_{n+1/2}(z)$ are simple and lie approximately along the left half of the boundary of an eye-shaped domain around $z = 0$ (see Figure* 2.1).

Proof. Properties (i) and (ii) can be found in [52, p. 511]. We now consider property (iii). As a consequence of (i), it suffices to consider the zeros of $K_\nu(z)$ in the third quadrant and on the negative real axis (i.e., with $-\pi \leq \arg z < -\pi/2$) of the complex plane. According to Formula 9.6.4 of [1], we have the following relation

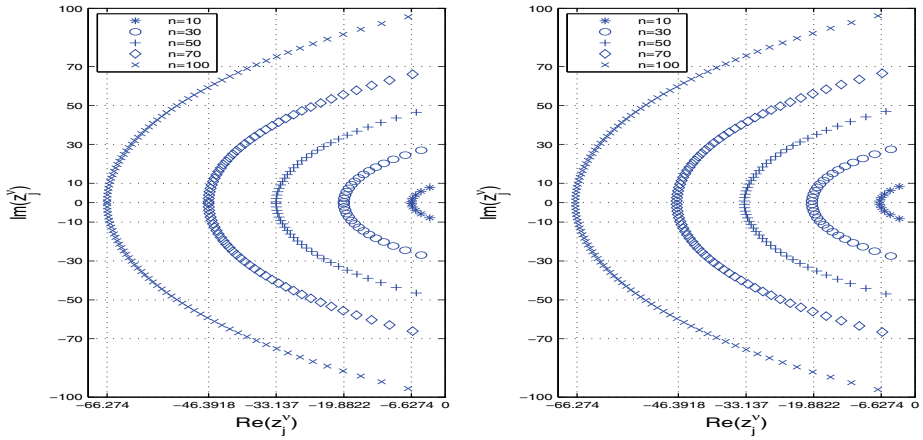

FIG. 2.1. *Distributions of $\{z_j^\nu\}_{j=1}^{M_\nu}$ of K_n (left) and $K_{n+1/2}$ (right) for various n.*

between $K_\nu(z)$ and the Hankel function of the first kind:

$$K_\nu(z) = \frac{\pi \mathrm{i}}{2} e^{\frac{1}{2}\nu\pi\mathrm{i}} H_\nu^{(1)}(\mathrm{i}z), \quad -\pi < \arg z \le \frac{\pi}{2}, \tag{2.17}$$

which implies that all zeros of $K_\nu(z)$ in the third quadrant (i.e., with $-\pi < \arg z < -\pi/2$) are obtained by rotating all zeros of $H_\nu^{(1)}(z)$ in the fourth quadrant (i.e., with $-\pi/2 < \arg z < 0$) by an angle $-\pi/2$. Recall that the zeros of $H_\nu^1(z)$ in the fourth quadrant lie approximately along the boundary of an eye-shaped domain around $z = 0$ (see Figure 9.6 and page 441 of [1]), whose boundary curve intersects the real axis at $z = n$ and the imaginary axis at $z = -\mathrm{i}na$, where $a = \sqrt{t_0^2 - 1} \approx 0.66274$ and $t_0 \approx 1.19968$ is the positive root of $\coth t = t$. □

For clarity, let M_ν be the total number of zeros of $K_\nu(z)$ with $\nu = n, n + 1/2$; that is,

$$M_\nu = \begin{cases} \text{the largest even integer nearest to } n - 1/2 & \text{for } K_n(z), \\ n & \text{for } K_{n+1/2}(z). \end{cases} \tag{2.18}$$

We plot in Figure 2.1 some samples of zeros of $K_n(z)$ and $K_{n+1/2}(z)$ for various n, and visualize that for a given n the zeros sit on the left half boundary of an eye-shaped domain that intersects the imaginary axis approximately at $\pm n\mathrm{i}$, and the negative real axis at $-na$ with $a \approx 0.66274$ (see the dashed coordinate grids), as predicted by Lemma 2.1(iii).

With the above understanding of the poles of the integrand $F_\nu(z)$ in (2.16), we now present the exact formula for the NRBKs $\sigma_\nu(t)$ with $\nu = n, n + 1/2$.

THEOREM 2.2. *Let $\nu = n, n + 1/2$ with $n \ge 0$, and let $\{z_j^\nu\}_{j=1}^{M_\nu}$ be the zeros of $K_\nu(z)$. Then*

- *for $d = 2$,*

$$\sigma_n(t) = \frac{c}{b^2} \left\{ \sum_{j=1}^{M_n} z_j^n e^{ctz_j^n/b} + (-1)^n \int_0^\infty \frac{e^{-ctr/b}}{K_n^2(r) + \pi^2 I_n^2(r)} dr \right\}; \tag{2.19}$$

- *for $d = 3$,*

$$\sigma_\nu(t) = \frac{c}{b^2} \sum_{j=1}^{M_\nu} z_j^\nu e^{ctz_j^\nu/b}, \quad \nu = n + \frac{1}{2}, \tag{2.20}$$

where $I_n(z)$ is the modified Bessel function of the first kind (cf. [1]).

We sketch the proof in Appendix A by applying the residue theorem to the Bromwich's contour integral (2.15). We remark that Sofronov [45] derived formulas of a similar type by working on much more complicated expressions in terms of Tricomi's confluent hypergeometric functions. However, the formulas in the above theorem are more compact and informative.

REMARK 2.2. *Based on a delicate study of the logarithmic derivative of the Hankel function $H_\nu^{(1)}(z)$, Alpert, Greengard, and Hagstrom* [2] (*see Theorem* 4.1 *and Lemma* 4.2 in [2]) *obtained the following formula:*

$$\begin{aligned} z\frac{H_\nu^{(1)'}(z)}{H_\nu^{(1)}(z)} &= \mathrm{i}z - \frac{1}{2} + \sum_{j=1}^{N_\nu} \frac{h_{\nu,j}}{z - h_{\nu,j}} \\ &\quad - \frac{1}{\pi\mathrm{i}} \int_0^\infty \frac{\pi\cos(\nu\pi)}{\cos^2(\nu\pi)K_\nu^2(r) + (\pi I_\nu(r) + \sin(\nu\pi)K_\nu(r))^2} \frac{1}{\mathrm{i}r + z} dr \end{aligned} \tag{2.21}$$

for any $\nu \neq n + 1/2$, *where* $h_{\nu,1}, h_{\nu,2}, \ldots, h_{\nu,N_\nu}$ *are zeros of* $H_\nu^{(1)}(z)$, *which number* N_ν. *Interestingly,* (2.19) *can be derived from* (2.21), *which is justified in Appendix* B.

REMARK 2.3. *Thanks to* (2.9), *we obtain from Theorem* 2.2 *the expression of* $\omega_\nu(t)$:

- *for* $d = 2$,
  (2.22)
  $$\omega_n(t) = -\frac{c}{2b} + \frac{c}{b}\left\{\sum_{j=1}^{M_n}\left(e^{ctz_j^n/b} - 1\right) + (-1)^n \int_0^\infty \frac{1 - e^{-ctr/b}}{r\{K_n^2(r) + \pi^2 I_n^2(r)\}} dr\right\};$$
- *for* $d = 3$,
  $$\omega_\nu(t) = -\frac{c}{b} + \frac{c}{b}\sum_{j=1}^{M_\nu}\left(e^{ctz_j^\nu/b} - 1\right), \quad \nu = n + \frac{1}{2}. \tag{2.23}$$

2.3. Computation of the improper integral in (2.19). The computation of the two-dimensional NRBK requires us to evaluate the improper integral involving the kernel function

$$W_n(r) := \frac{1}{K_n^2(r) + \pi^2 I_n^2(r)} := \frac{1}{G_n(r)}, \quad n \geq 0, \ \ r > 0, \tag{2.24}$$

whose important properties are characterized below.

LEMMA 2.3. *For any* $n \geq 0$ *and any real* $r > 0$, *we have that*

(i) $G_n(r)$ *is a convex function on the positive real axis, and* $W_n(r)$ *attains its maximum at a unique point;*

(ii) *for large* n, *we have the uniform asymptotic estimate*

$$W_n(n\kappa) \sim \frac{n\sqrt{1+\kappa^2}}{\pi}\operatorname{sech}(2n\Theta) := \widetilde{W}_n(n\kappa), \quad \kappa > 0, \tag{2.25}$$

where

$$\Theta = \Theta(\kappa) := \sqrt{1+\kappa^2} + \ln\frac{\kappa}{1+\sqrt{1+\kappa^2}}. \tag{2.26}$$

Approximately, the maximum value of $W_n(r)$ *is attained at* $r = na$ *with* $a \approx 0.66274$ *being the root of* Θ, *and the maximum value is approximately* $n\sqrt{1+a^2}/\pi \approx 0.38187n$.

Proof. (i) We find from page 374 of [1] that for a given n, $K_n(r), I_n(r) > 0$, and $K_n(r)$ (resp., $I_n(r)$) is monotonically descending (resp., ascending) with respect to r. From the series representation (see Formula 9.6.10 of [1]),

$$I_n(r) = \frac{r^n}{2^n}\sum_{k=0}^{\infty}\frac{r^{2k}}{2^{2k}k!(n+k)!}, \quad n \geq 0,$$

we conclude that $I_n''(r) > 0$. Moreover, since $K_n(r)$ satisfies (see Formula 9.6.1 of [1])

$$r^2K_n''(r) + rK_n'(r) - (r^2 + n^2)K_n(r) = 0,$$

we have $K_n''(r) > 0$. Therefore, a direct calculation shows that $G_n''(r) > 0$, so $G_n(r)$ is convex.

One verifies that $G_n(0+) = G_n(+\infty) = +\infty$ for all n, which follows from

$$K_\nu(r) \sim \sqrt{\frac{\pi}{2r}} e^{-r} \left\{ 1 + \frac{4\nu^2 - 1}{8r} + O(r^{-2}) \right\}$$

(cf. (2.12)), and the asymptotic properties (see [1] again)

$$K_\nu(r) \sim \begin{cases} -\ln r & \text{if } \nu = 0, \\ \dfrac{\Gamma(\nu)}{2} \Big(\dfrac{r}{2}\Big)^{-\nu} & \text{if } \nu > 0, \end{cases} \qquad I_\nu(r) \sim \frac{1}{\Gamma(\nu+1)} \Big(\frac{r}{2}\Big)^{\nu}, \quad \nu \geq 0, \tag{2.27}$$

for $0 < r \ll 1$, and

$$I_\nu(r) \sim \sqrt{\frac{1}{2\pi r}} e^{r}, \quad r \gg 1, \quad \nu \geq 0. \tag{2.28}$$

Since $G_n(r)$ is convex, $G_n(r)$ attains its minimum at a unique point r_0. Thanks to $G_n'(r) = -W_n'(r)/W_n^2(r)$, $W_n(r)$ has a unique maximum at the same point r_0.

(ii) Recall that for large n (see Formulas (9.7.7)–(9.7.11) of [1]),

$$\begin{aligned} K_n(n\kappa) &\sim \sqrt{\frac{\pi}{2n}} \frac{e^{-n\Theta}}{(1+\kappa^2)^{1/4}}, & I_n(n\kappa) &\sim \frac{1}{\sqrt{2\pi n}} \frac{e^{n\Theta}}{(1+\kappa^2)^{1/4}}, \\ K_n'(n\kappa) &\sim -\sqrt{\frac{\pi}{2n}} \frac{(1+\kappa^2)^{1/4}}{\kappa} e^{-n\Theta}, & I_n'(n\kappa) &\sim \frac{1}{\sqrt{2\pi n}} \frac{(1+\kappa^2)^{1/4}}{\kappa} e^{n\Theta}, \end{aligned} \tag{2.29}$$

which, together with (2.24), lead to the asymptotic estimate (2.25). Thus, the maximum value of $W_n(r)$ is approximately attained at the unique root of $\Theta(\kappa)$, which turns out to be $a \approx 0.66274$ as in Figure 2.1, and the maximum value is about $n\sqrt{1+a^2}/\pi \approx 0.38187n$. ∎

We depict in Figure 2.2 (left) the graph of $\Theta(\kappa)$ and highlight the zero point $(a, 0)$. Observe that $\Theta(\kappa)$ grows like κ when $\kappa > a$. We plot in Figure 2.2 (right) several sample graphs of W_n (solid lines) and the asymptotic estimate $\widetilde{W}_n$ ("•"), and particularly mark the asymptotic point $(na, n\sqrt{1+a^2}/\pi)$ of the maximum of $W_n(r)$

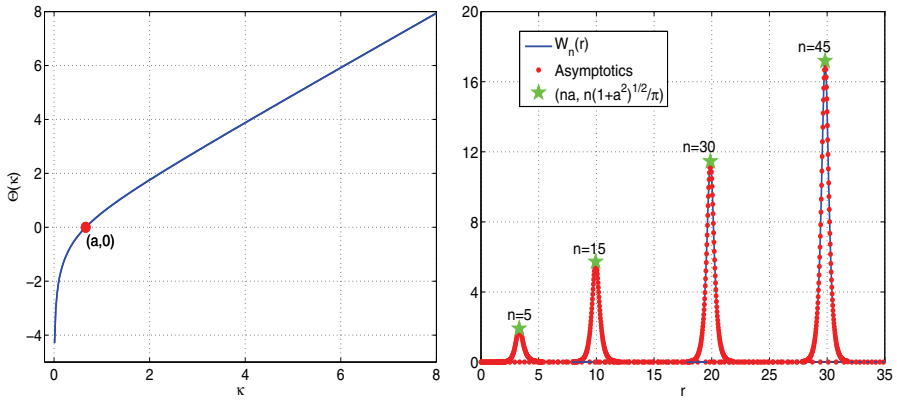

FIG. 2.2. *Left: graph of* $\Theta(\kappa), \kappa \in (0, 8]$ *defined in* (2.26). *Right:* W_n *against the asymptotic estimate* $\widetilde{W}_n$ ("•") *for* $n = 5, 15, 30, 45$.

obtained in Lemma 2.3(ii). Observe that even for small n, the asymptotic estimate provides a very accurate approximation of W_n.

As $W_n(r)$ behaves like a spike, we can truncate the improper integral in (2.19) and approximate it very accurately. For $n \geq n_0$ (e.g., $n_0 = 8$ in our computation), we truncate $(0, \infty)$ to a narrow interval $[L_1, L_2] := [(a - \delta_1)n, (a + \delta_2)n]$ around the maximum point $r = na$, where δ_1 and δ_2 are chosen such that for a preassigned tolerance $\varepsilon > 0$, $\delta_1 = \sup_\delta \widetilde{W}_n((a - \delta)n) < \varepsilon$ and $\delta_2 = \inf_\delta \widetilde{W}_n((a + \delta)n) < \varepsilon$. For small $n < n_0$, we simply take $L_1 = 0$ and choose $L_2 = \inf_r W_n(r) < \varepsilon$. We tabulate in Table 2.1 the truncated interval with $\varepsilon = 10^{-13}$ for various n and see that the length of the interval of interest is around 18. For the reader's reference, we provide in Table 2.2 some samples of $\sigma_n(t)$ with $b = c = 1$.

TABLE 2.1
Truncation of the improper integral.

n	L_1	L_2	$L_2 - L_1$	n	L_1	L_2	$L_2 - L_1$	n	L_1	L_2	$L_2 - L_1$
0	0	16.1	16.1	8	0.81	18.0	17.2	30	12.2	30.5	18.3
2	0	16.3	16.3	10	1.49	18.9	17.4	40	18.4	36.9	18.5
4	0	16.7	16.7	15	3.71	21.4	17.7	50	24.8	43.5	18.7
6	0	17.2	17.2	20	6.35	24.3	18.0	60	31.2	50.2	19.0

TABLE 2.2
Some samples of $\sigma_n(t)$.

n	$\sigma_n(0)$	$\sigma_n(1)$	$\sigma_n(2)$	$\sigma_n(3)$
0	1.250000000000e-1	5.684288622608e-2	3.351856052343e-2	2.266050114914e-2
5	-1.237500000000e+1	2.202467951276e-1	-4.319989183539e-2	5.379927213148e-3
10	-4.987500000000e+1	-7.484612960447e-1	7.405362971595e-3	1.794812888151e-3
30	-4.498750000000e+2	-4.436774439706e-1	2.776460499307e-3	2.472420517813e-5
80	-3.199875000000e+3	-9.903043482030e-2	-1.941146013844e-4	-2.697087894087e-7
120	-7.199875000000e+3	-7.499180003657e-2	4.237771379095e-5	-8.100282555699e-9

2.4. Rapid evaluation of the temporal convolution. The presence of the time variable t in the exponentials in (2.19) and (2.20) allows us to eliminate the burden of history dependence of temporal convolution as in [3]. More precisely, given a function $g(t)$, we define

$$f(t; r) := e^{-ctr/b} * g(t) = \int_0^t e^{-c(t-\tau)r/b} g(\tau) d\tau.$$

One verifies readily that

$$f(t + \Delta t; r) = e^{-c\Delta t r/b} f(t; r) + \int_t^{t+\Delta t} e^{-c(t+\Delta t-\tau)r/b} g(\tau) d\tau, \tag{2.30}$$

so $f(t; r)$ can march in t with step size Δt recursively. This enables us to compute the time convolution rapidly. For example, in the two-dimensional case,

$$\begin{aligned}
[\sigma_n * g](t) &= \int_0^t \sigma_n(t - \tau) g(\tau) d\tau = \frac{c}{b^2} \sum_{j=1}^{M_n} z_j^n \int_0^t e^{c(t-\tau) z_j^n / b} g(\tau) d\tau \\
&\quad + \frac{(-1)^n c}{b^2} \int_0^\infty \frac{1}{K_n^2(r) + \pi^2 I_n^2(r)} \left[\int_0^t e^{-c(t-\tau)r/b} g(\tau) d\tau \right] dr \qquad (2.31) \\
&= \frac{c}{b^2} \sum_{j=1}^{M_n} z_j^n f(t; -z_j^n) + \frac{(-1)^n c}{b^2} \int_0^\infty f(t; r) W_n(r) dr.
\end{aligned}$$

Thanks to (2.30), $[\sigma_n * g](t+\Delta t)$ can be computed recursively from the previous step, and the history dependence is then narrowed down to $[t, t+\Delta t]$. We also refer the reader to subsections 4.4–4.5 for more detailed discussions.

3. A priori estimates. In this section, we analyze the well-posedness of the truncated problem (2.4)–(2.6) and provide a priori estimates for its solution.

We first recall the Plancherel or Parseval results for the Laplace transform.

LEMMA 3.1. *Let $s = s_1 + \mathrm{i}s_2$ with $s_1, s_2 \in \mathbb{R}$. If f, g are Laplace transformable, then*

$$\frac{1}{2\pi}\int_{-\infty}^{\infty} \mathcal{L}[f](s)\,\mathcal{L}[\bar{g}](s)\,ds_2 = \int_0^{\infty} e^{-2s_1 t} f(t)\bar{g}(t)dt \quad \forall\, s_1 > \gamma, \tag{3.1}$$

where γ is the abscissa of convergence for both f and g, and $\bar{g}$ is the complex conjugate of g.

Proof. This identity can be proved by following along the same lines as those for (2.46) in [12] (or [16]). ∎

For notational convenience, we introduce the modified spherical Bessel function (cf. [52])

$$k_n(z) = \sqrt{\frac{2}{\pi z}} K_{n+1/2}(z) \;\Rightarrow\; \frac{k_n'(z)}{k_n(z)} = -\frac{1}{2z} + \frac{K_{n+1/2}'(z)}{K_{n+1/2}(z)}, \tag{3.2}$$

and by (2.11),

$$\omega_{n+1/2}(t) = \mathcal{L}^{-1}\left[1 + \frac{k_n'(sb/c)}{k_n(sb/c)}\right](t), \quad n \geq 0. \tag{3.3}$$

The following properties are also indispensable for the analysis.

LEMMA 3.2. *Let $s = s_1 + \mathrm{i}s_2$ with $s_1, s_2 \in \mathbb{R}$. Then for any $s_1 > 0$,*

(3.4)

$$\text{(i) } \mathrm{Re}\left(s\frac{Z_n'(sb/c)}{Z_n(sb/c)}\right) \leq 0,\;\; \mathrm{Re}\left(\frac{Z_n'(sb/c)}{Z_n(sb/c)}\right) \leq 0;\;\; \text{(ii) } \mathrm{Im}\left(s\frac{Z_n'(sb/c)}{Z_n(sb/c)}\right) \leq 0 \;\; \forall s_2 \geq 0,$$

where $Z_n(z) = K_n(z)$ or $k_n(z)$.

Proof. The results with $Z_n = K_n$ were proved in Chen [9]. We next prove (3.4) with $Z_n = k_n$ by using a similar argument. By applying Laplace transform to (2.1)–(2.3), exterior to $D = B$ with $F = U_0 = U_1 \equiv 0$ and $G = U|_{r=b}$, and denoting $u = \mathcal{L}[U]$, we obtain

$$\begin{aligned} &-c^2\Delta u + s^2 u = 0 \quad \text{in } \Omega_{\mathrm{ext}} = \mathbb{R}^d \setminus \bar{B},\;\; s \in \mathbb{C},\;\; \mathrm{Re}(s) > 0; \\ &u|_{r=b} = \psi = \mathcal{L}[U|_{r=b}]; \quad c\partial_r u + su = o\big(r^{(1-d)/2}\big),\;\; d = 2, 3, \end{aligned} \tag{3.5}$$

which admits the series solution

$$u(r,\theta,\phi,s) = \sum_{n=0}^{\infty} \frac{k_n(sr/c)}{k_n(sb/c)} \sum_{|m|=0}^{n} \hat{\psi}_{nm}(s) Y_n^m(\theta,\phi), \tag{3.6}$$

where $\{\hat{\psi}_{nm}\}$ are the spherical harmonic expansion coefficients of ψ. Multiplying the first equation of (3.5) by $\bar{u}$ and integrating over $\Omega_{b,\rho} := B_\rho \setminus \bar{B}$, where B_ρ is a ball of radius $\rho > b$, the imaginary part of the resulting equation reads as

$$2s_1 s_2 \int_{\Omega_{b,\rho}} |u|^2 d\boldsymbol{x} - c^2\,\mathrm{Im}\int_{\partial\Omega_{b,\rho}} \frac{\partial u}{\partial \boldsymbol{n}}\bar{u}\,d\gamma = 0, \tag{3.7}$$

where $\boldsymbol{n}$ is the unit outer normal of $\partial\Omega_{b,\rho}$.

Since $s_1 > 0$, multiplying (3.7) by s_2 yields

$$s_2 \,\mathrm{Im} \int_{\{r=b\}} \frac{\partial u}{\partial r} \bar{u}\, d\gamma \le s_2 \,\mathrm{Im} \int_{\{r=\rho\}} \frac{\partial u}{\partial r} \bar{u}\, d\gamma. \tag{3.8}$$

It is clear that $u = k_n(sr/c)/k_n(sb/c)\hat{\psi}_{nm}(s)Y_n^m(\theta,\phi)$ is a solution of (3.5), so using the orthogonality of $\{Y_n^m\}$ and the fact $\bar{k}_n/|k_n|^2 = 1/k_n$, we obtain from (3.8) that

$$\frac{b}{c}\mathrm{Im}\left(s_2 s \frac{k_n'(sb/c)}{k_n(sb/c)}\right)|\hat{\psi}_{nm}|^2 \le \frac{\rho}{c}\mathrm{Im}\left(s_2 s \frac{k_n'(s\rho/c)}{k_n(sb/c)}\right)|\hat{\psi}_{nm}|^2. \tag{3.9}$$

We find from (2.12) and (3.2) that $k_n'(s\rho/c)$ decays exponentially if $s_1 > 0$, so the right-hand side of (3.8) tends to zero as $\rho \to +\infty$. Thus, letting $\rho \to +\infty$ in (3.9) leads to

$$\mathrm{Im}\left(s_2 s \frac{k_n'(sb/c)}{k_n(sb/c)}\right) \le 0. \tag{3.10}$$

If $s_2 \ge 0$, we obtain (ii) in (3.4). Next, we prove the first inequality of (i) in (3.4). Recall the formula (see Lemma 2.3 of [9])

$$|K_{n+1/2}(sr)|^2 = \frac{1}{2}\int_0^\infty e^{-\frac{|s|^2 r^2}{2\tau} - \frac{s^2+\bar{s}^2}{2|s^2|}} K_{n+1/2}(\tau)\frac{d\tau}{\tau}, \quad s_1 > 0,$$

which implies that $|K_{n+1/2}(sr)|^2$ is monotonically descending with respect to r. The property $\frac{d}{dr}|K_{n+1/2}(sr)|^2 \le 0$, together with (3.2), implies $\mathrm{Re}\big(s\frac{k_n'(sb/c)}{k_n(sb/c)}\big) \le 0$. Denoting $s\frac{k_n'(sb/c)}{k_n(sb/c)} = \gamma_1 + \mathrm{i}\gamma_2$ with $\gamma_1, \gamma_2 \in \mathbb{R}$, we know from (3.10) that $\gamma_1 \le 0$ and $s_2\gamma_2 \le 0$. Therefore,

$$\mathrm{Re}\left(\frac{k_n'(sb/c)}{k_n(sb/c)}\right) = \mathrm{Re}\left(\frac{\gamma_1 + \mathrm{i}\gamma_2}{s}\right) = \frac{1}{|s|^2}(s_1\gamma_1 + s_2\gamma_2) \le 0.$$

This ends the proof. ∎

With the above preparations, we can derive the following important property.

THEOREM 3.3. *For any $v \in L^2(0,T)$, we have*

$$\mathrm{Re}\int_0^T [\omega_\nu * v](t)\bar{v}(t)dt \le \int_0^T |v(t)|^2 dt \quad \forall\, T > 0,\ \ n \ge 0, \tag{3.11}$$

where ω_ν is the NRBK given by (2.11) (*or* (3.3) *for $d = 3$*).

Proof. Let $\tilde{v} = v\,\mathbf{1}_{[0,T]}$, where $\mathbf{1}_{[0,T]}$ is the characteristic function of $[0,T]$. Then we obtain from (3.1) that for $d = 3$,

$$\begin{aligned}
\int_0^T e^{-2s_1 t}[\omega_{n+1/2} * v](t)\bar{v}(t)dt &= \int_0^\infty e^{-2s_1 t}[\omega_{n+1/2} * \tilde{v}](t)\bar{\tilde{v}}(t)dt \\
&= \frac{1}{2\pi}\int_{-\infty}^\infty \left[\frac{k_n'(sb/c)}{k_n(sb/c)} + 1\right]\big|\mathcal{L}[\tilde{v}](s)\big|^2 ds_2 \\
&= \frac{1}{2\pi}\int_{-\infty}^\infty \frac{k_n'(sb/c)}{k_n(sb/c)}\big|\mathcal{L}[\tilde{v}](s)\big|^2 ds_2 + \frac{1}{2\pi}\int_{-\infty}^\infty \big|\mathcal{L}[\tilde{v}](s)\big|^2 ds_2.
\end{aligned}$$

It is clear that by (3.1) with $f = g = \tilde{v}$,

$$\frac{1}{2\pi}\int_{-\infty}^\infty \big|\mathcal{L}[\tilde{v}](s)\big|^2 ds_2 = \int_0^{+\infty} e^{-2s_1 t}|\tilde{v}(t)|^2 dt = \int_0^T e^{-2s_1 t}|v(t)|^2 dt.$$

On the other hand, we have

$$\begin{aligned}\frac{1}{2\pi}\mathrm{Re}\int_{-\infty}^{\infty}\frac{k_n'(sb/c)}{k_n(sb/c)}\big|\mathcal{L}[\tilde v](s)\big|^2ds_2 &= \frac{1}{2\pi}\int_{-\infty}^{\infty}\mathrm{Re}\left(\frac{k_n'(sb/c)}{k_n(sb/c)}\right)\big|\mathcal{L}[\tilde v](s)\big|^2ds_2\\ &= \frac{1}{2\pi}\int_{-\infty}^{\infty}\mathrm{Re}\left(\frac{k_n'(sb/c)}{k_n(sb/c)}\right)\left|\mathcal{L}\left[\int_0^t\tilde v(\tau)d\tau\right](s)\right|^2|s|^2ds_2.\end{aligned}\tag{3.12}$$

Thus, we conclude from Lemma 3.2 and the above identities that for $s_1>0$,

$$\mathrm{Re}\int_0^T e^{-2s_1t}[\omega_{n+1/2}*v](t)\bar v(t)dt\le\int_0^T e^{-2s_1t}|v(t)|^2dt.\tag{3.13}$$

Notice that the asymptotic formulas in (2.27) are also valid for complex r (see Formula 9.6.9 in [1]), which, together with Lemma 2.1, implies that $k_n'(sb/c)/k_n(sb/c)$ is analytic for all $\mathrm{Re}(s)\ge 0$ but $|s|\neq 0$, and $\lim_{s_1\to 0^+}|s|^2k_n'(sb/c)/k_n(sb/c)$ exists for all s_2. Hence, the integral in (3.12) is finite. Letting $s_1\to 0^+$ in (3.13) leads to the desired result for $d=3$.

The result (3.11) with $d=2$ can be proved in a similar fashion. ∎

COROLLARY 3.4. *Suppose that $v'\in L^2(0,T)$ with $v(0)=0$. Then we have*

$$\mathrm{Re}\int_0^T[\sigma_\nu*v](t)\bar v'(t)dt\le\frac{1}{c}\int_0^T|v'(t)|^2dt+\frac{d-1}{4b}|v(T)|^2\quad\forall\,T>0\tag{3.14}$$

for $\nu=n,n+1/2$, where $\sigma_\nu(t)$ is the NRBK defined in (2.8).

Proof. By (2.9), we have $\omega_\nu'(t)=c\sigma_\nu(t)$, $\omega_\nu(0)=-\frac{(d-1)c}{2b}$. Thus, we obtain from integration by parts and the fact $v(0)=0$ that

$$[\omega_\nu*v'](t)=-\frac{(d-1)c}{2b}v(t)+c[\sigma_\nu*v](t).$$

By Theorem 3.3 with v' in place of v,

$$\begin{aligned}\mathrm{Re}\int_0^T[\omega_\nu*v'](t)\bar v'(t)dt &= -\frac{(d-1)c}{2b}\,\mathrm{Re}\int_0^Tv(t)\bar v'(t)dt+c\,\mathrm{Re}\int_0^T[\sigma_\nu*v](t)\bar v'(t)dt\\ &= -\frac{(d-1)c}{4b}|v(T)|^2+c\,\mathrm{Re}\int_0^T[\sigma_\nu*v](t)\bar v'(t)dt\le\int_0^T|v'(t)|^2dt.\end{aligned}$$

This gives (3.14). ∎

Now, we are ready to analyze the stability of the solution of the truncated problem (2.4)–(2.6). To this end, we assume that the scatterer D is a simply connected domain with Lipschitz boundary Γ_D, and the Dirichlet data $G=0$ on Γ_D. More precisely, the problem of interest is

$$\partial_t^2U=c^2\Delta U+F\quad\text{in }\Omega:=B\setminus\bar D,\ \ t>0,\ \ d=2,3;\tag{3.15}$$

$$U=U_0,\quad\partial_tU=U_1\quad\text{in }\Omega,\ \ t=0;\quad U=0\quad\text{on }\Gamma_D,\ \ t>0;\tag{3.16}$$

$$\partial_rU-T_d(U)=H\quad\text{at }\ r=b,\ \ t>0,\tag{3.17}$$

where the given data H may result from lifting of nonhomogeneous Dirichlet data or from the boundary perturbation to be described in subsection 4.1. Denote $X:=\big\{U\in H^1(\Omega):U|_{\Gamma_D}=0\big\}$, and let $(\cdot,\cdot)_{L^2(\Omega)}$ and $\|\cdot\|_{L^2(\Omega)}$ be the inner product and

norm of $L^2(\Omega)$, respectively, and likewise, we define $\langle\cdot,\cdot\rangle_{L^2(\Gamma_b)}$ and $\|\cdot\|_{L^2(\Gamma_b)}$, where $\Gamma_b=\{r=b\}$ and b is the radius of the artificial boundary.

THEOREM 3.5. *Let $U(\in X)$ be the solution of (3.15)–(3.17). If $U_0\in H^1(\Omega), U_1\in L^2(\Omega), H\in L^\infty(0,T;L^2(\Gamma_b)), \partial_t H\in L^1(0,T;L^2(\Gamma_b))$, and $F\in L^1(0,T;L^2(\Omega))$ for any $T>0$, then we have $\nabla U\in L^\infty(0,T;(H^1(\Omega))^d)$, $\partial_t U\in L^\infty(0,T;L^2(\Omega))$, and there holds*

$$\begin{aligned}(3.18)\quad &\|\partial_t U\|_{L^\infty(0,T;L^2(\Omega))}+c\|\nabla U\|_{L^\infty(0,T;L^2(\Omega))}\le C\big(\|U_1\|_{L^2(\Omega)}+c\|\nabla U_0\|_{L^2(\Omega)}\\ &\qquad+\|H\|_{L^\infty(0,T;L^2(\Gamma_b))}+\|\partial_t H\|_{L^1(0,T;L^2(\Gamma_b))}+\|F\|_{L^1(0,T;L^2(\Omega))}\big),\end{aligned}$$

where C is a positive constant independent of any functions and c. Moreover, if $F\equiv 0$ and $H\equiv 0$, we have the conservation of the energy: $E'(t)=0$ for all $t\ge 0$, where

$$(3.19)\qquad E(t)=\int_\Omega\big(|\partial_t U|^2+c^2|\nabla U|^2\big)d\boldsymbol{x}-2c^2\int_0^t\int_{\Gamma_b}T_d(U)\partial_\tau\overline{U}d\gamma d\tau.$$

Proof. Multiplying (3.15) by $2\partial_t\overline{U}$, integrating over Ω, and taking the real part of the resulting equation, we derive from the Green's formula that for any $t>0$,

$$\begin{aligned}(3.20)\quad &\frac{d}{dt}\Big(\|\partial_t U\|^2_{L^2(\Omega)}+c^2\|\nabla U\|^2_{L^2(\Omega)}\Big)-2c^2\,\mathrm{Re}\int_{\Gamma_b}T_d(U)\partial_t\overline{U}d\gamma\\ &\qquad=2\mathrm{Re}(F,\partial_t U)_{L^2(\Omega)}+2c^2\,\mathrm{Re}\langle H,\partial_t U\rangle_{\Gamma_b}.\end{aligned}$$

Integrating the above equation over $(0,t)$, we find that for any $t>0$,

$$\begin{aligned}&\|\partial_t U\|^2_{L^2(\Omega)}+c^2\|\nabla U\|^2_{L^2(\Omega)}-2c^2\,\mathrm{Re}\int_0^t\int_{\Gamma_b}T_d(U)\partial_\tau\overline{U}d\gamma d\tau\\ &=2\,\mathrm{Re}\int_0^t(F,\partial_\tau U)_{L^2(\Omega)}d\tau+2c^2\,\mathrm{Re}\int_0^t\langle H,\partial_\tau U\rangle_{\Gamma_b}d\tau+\|U_1\|^2_{L^2(\Omega)}+c^2\|\nabla U_0\|^2_{L^2(\Omega)}\\ &\le 2\|\partial_t U\|_{L^\infty(0,T;L^2(\Omega))}\|F\|_{L^1(0,T;L^2(\Omega))}\\ &\qquad+2c^2\,\mathrm{Re}\int_0^t\langle H,\partial_\tau U\rangle_{\Gamma_b}d\tau+\|U_1\|^2_{L^2(\Omega)}+c^2\|\nabla U_0\|^2_{L^2(\Omega)}.\end{aligned}$$

Using integration by parts leads to

$$\begin{aligned}(3.21)\quad &\mathrm{Re}\int_0^t\langle H,\partial_\tau U\rangle_{\Gamma_b}d\tau=\mathrm{Re}\langle H,U\rangle_{\Gamma_b}-\mathrm{Re}\langle H,U\rangle_{\Gamma_b}\big|_{t=0}-\mathrm{Re}\int_0^t\langle\partial_\tau H,U\rangle_{\Gamma_b}d\tau\\ &\le 2\|H\|_{L^\infty(0,T;L^2(\Gamma_b))}\|U\|_{L^\infty(0,T;L^2(\Gamma_b))}+\|\partial_t H\|_{L^1(0,T;L^2(\Gamma_b))}\|U\|_{L^\infty(0,T;L^2(\Gamma_b))}\\ &\le C\big(\|H\|_{L^\infty(0,T;L^2(\Gamma_b))}+\|\partial_t H\|_{L^1(0,T;L^2(\Gamma_b))}\big)\|\nabla U\|_{L^\infty(0,T;L^2(\Omega))},\end{aligned}$$

where we used the following estimate derived from the trace inequality (see, e.g., [7, eq. (1.6.2)]) and the Poincaré inequality (see, e.g., [10, Theorem 1.2.1]):

$$\|U\|_{L^\infty(0,T;L^2(\Gamma_b))}\le C\|U\|^{1/2}_{L^\infty(0,T;L^2(\Omega))}\|U\|^{1/2}_{L^\infty(0,T;H^1(\Omega))}\le C\|\nabla U\|_{L^\infty(0,T;L^2(\Omega))}.$$

We next show that for any $t>0$,

$$(3.22)\qquad \mathrm{Re}\int_0^t\int_{\Gamma_b}T_d(U)\partial_\tau\overline{U}d\gamma d\tau\le 0.$$

For $d = 3$, it follows from (2.10), Theorem 3.3, and the orthogonality of $\{Y_n^m\}$ that

$$\begin{aligned}\mathrm{Re}\int_0^t\int_{\Gamma_b} T_d(U)\partial_\tau\overline{U}d\gamma d\tau &= -\frac{1}{c}\int_0^t \|\partial_\tau U\|^2_{L^2(\Gamma_b)}d\tau\\ &\quad+\frac{1}{c}\sum_{n=0}^{\infty}\sum_{|m|=0}^{n}\mathrm{Re}\int_0^t\big[\omega_{n+1/2}*\partial_\tau\widehat{U}_{nm}(b,\tau)\big]\partial_\tau\overline{\widehat{U}}_{nm}(b,\tau)d\tau\\ &\overset{(3.11)}{\le} -\frac{1}{c}\int_0^t \|\partial_\tau U\|^2_{L^2(\Gamma_b)}d\tau+\frac{1}{c}\sum_{n=0}^{\infty}\sum_{|m|=0}^{n}\int_0^t\big|\partial_\tau\widehat{U}_{nm}(b,\tau)\big|^2d\tau=0.\end{aligned}$$

This verifies (3.22) with $d = 3$. Similarly, one can justify (3.22) with $d = 2$.

Consequently, the estimate (3.18) follows from (3.20)–(3.21) and the Cauchy–Schwarz inequality.

Letting $F \equiv 0$ and $H \equiv 0$ in (3.21) leads to the conservation of energy. ∎

REMARK 3.1. *Note that* (i) *if $T_d(U)$ is given by* (2.7)*, we can use Corollary* 3.4 *to verify* (3.22)*;* (ii) *a similar estimate for $d = 2$ was derived by* [9] *with a slightly different argument; and* (iii) *it is seen from* (3.18) *that the validation of this estimate requires $\partial_t H \in L^1(0,T;L^2(\Gamma_b))$, which appears restrictive. This is largely due to the lack of the uniform Kreiss–Lopatinski conditions* (*cf.* [40]) *for the truncated wave equation* (*also refer to the appendix of* [2]).

4. Spectral-Galerkin approximation and Newmark's time integration. This section is devoted to numerical approximation of the truncated problem (2.4)–(2.6) with a focus on the treatment for the global NRBC imposed at the circular/spherical boundary $r = b$. Given the series representation of the NRBC in (2.7), it is known that if the scatterer D is a disk/ball (i.e., the computational domain Ω is an annulus or a spherical shell), the NRBC in space becomes local in the space of Fourier/spherical harmonic coefficients. The use of polar/spherical coordinates allows us to reduce the truncated problem to a sequence of decoupled one-dimensional problems (see (4.3) below), which therefore leads to fast spatial Fourier/spherical harmonic-Legendre spectral solvers. It is due to this fact that efficient spectral-Galerkin methods integrated with a boundary perturbation technique have been successfully applied to simulate the time-harmonic acoustic scattering waves by an irregular bounded obstacle with moderate to large wave numbers (see, e.g., [35, 18]). The boundary perturbation method (sometimes termed the "method of variation of boundary") had its roots in the monumental works of Rayleigh [37] and Rice [38], with a flurry of subsequent improvements and enhancements (cf. Bruno and Reitich [8] and Nicholls and Reitich [34]). Within its domain of applicability, this method is fast and accurate, and in particular, an enhanced version, called the transformed field expansion (TFE) method, has proved to be robust for large and/or rough boundary perturbations. The key to success lies in the convergence property that "the scattered field depends analytically on the domain perturbations under reasonable assumptions on the geometry of the scatterer surface and regularity of boundary data" (see [36] for a rigorous analysis). While the major requisite pieces are in order for frequency-domain computation, the process of assembling them to design high-order time-domain methods is far from trivial. Here we intend to construct one of the major building blocks, that is, the efficient space-time solver for (2.4)–(2.6) in an annulus or a spherical shell, but we leave the combination with the TFE method to a future work as the implementation is rather involved.

4.1. Notion of TFE. We outline this technique for (2.4)–(2.6) with $d = 2$ and

$$\Gamma_D = \big\{r = b_0 + \eta(\phi) : 0 \le \phi < 2\pi\big\}, \quad b > b_0 + \max_{\phi\in[0,2\pi]} |\eta(\phi)|,$$

where $r(\phi) = b_0 + \eta(\phi)$ is the parametric form of the boundary of the scatterer D. As before, the outer artificial disk $\{r = b\}$ contains the scatterer D and supports of the source term and initial data. Based on the general setup for the TFE method in [36], we assume that η is smooth (in certain Sobolev space with regularity index $\ge 3/2$ in Theorem 5.5 of [36]) and assume that the domain Ω is "close" to a regular simple domain Ω_0.

- As the name suggests, we first make a change of variables,

$$r' = \frac{(b - b_0)r - b\eta(\phi)}{(b - b_0) - \eta(\phi)}, \quad \phi' = \phi,$$

which maps Ω to the annulus $\Omega_0 = \big\{(r', \phi') : b_0 < r' < b,\ 0 \le \phi' < 2\pi\big\}$. To simplify the notation, we still use U, F, r, ϕ, etc. to denote the transformed functions or variables. Then the problem (2.4)–(2.6) becomes

$$\begin{aligned}
&\partial_t^2 U = c^2\Delta U + F + J(\eta, U) \ \text{ in } \ \Omega_0, \ \ t > 0;\\
&U = U_0, \ \ \partial_t U = U_1 \ \text{ in } \ \Omega_0, \ \ t = 0;\\
&U|_{r=b_0} = G, \quad t > 0; \ \ \big(\partial_r U - T_d(U)\big)|_{r=b} = L(\eta, U)|_{r=b}, \quad t > 0,
\end{aligned}$$

where $J(\eta, U)$ and $L(\eta, U)$ contain differential operators with nonconstant coefficients.

- Considering the smooth boundary deformation $\eta = \varepsilon\zeta$, the scattering field, U, has the strongly convergent expansion

$$U(r, \phi, t; \varepsilon) = \sum_{l=0}^{\infty} U_l(r, \phi, t)\varepsilon^l, \quad t > 0, \tag{4.1}$$

which depends analytically on ε. Formally, by expanding the data in a similar series, we obtain the sequence of equations after collecting the terms of ε^l (similar to the derivations in [35]):

$$\begin{aligned}
&\partial_t^2 U_l = c^2\Delta U_l + F_l + \tilde{J}(\eta, U_{l-4}, \ldots, U_{l-1}) \quad \text{in } \ \Omega_0, \ \ t > 0;\\
&U_l = U_{0,l}, \quad \partial_t U_l = U_{1,l} \quad \text{in } \ \Omega_0, \ \ t = 0;\\
&U_l|_{r=b_0} = G_l, \quad t > 0; \quad \big(\partial_r U_l - T_d(U_l)\big)|_{r=b} = \tilde{L}(\eta, U_{l-1})|_{r=b}, \quad t > 0.
\end{aligned}$$

- We solve the above equation for $l = 0, 1, \ldots$, and sum up the series by using a Padé approximation.

We remark that the parameter ε, which measures the size of perturbation, does not have to be small [34], and numerical evidence in [35] shows that the method in the frequency-domain produces satisfactory results for the very rough scatterer of Lipschitz C^0 (star-like) shape. We also point out that in this context, we have extra time derivatives in the functionals $\tilde{J}$ and $\tilde{L}$. Under this notion, the whole algorithm boils down to solving a sequence of prototype equations, so it becomes crucial to develop a fast, stable solver for the problem (4.2) below.

4.2. Prototype equation and dimension reduction. Consider

$$\begin{aligned}
&\partial_t^2 U = c^2\Delta U + F \quad \text{in } \Omega_0 = \big\{\boldsymbol{x}\in\mathbb{R}^d : b_0 < |\boldsymbol{x}| < b\big\},\ \ t>0;\\
&U = U_0,\ \ \partial_t U = U_1 \ \text{ in } \Omega_0,\ \ t=0;\\
&U|_{r=b_0} = 0, \quad \big(\partial_r U - T_d(U)\big)\big|_{r=b} = H,\ \ t>0,
\end{aligned} \tag{4.2}$$

where $T_d(U)$ is the DtN map as before. By expanding the solution and expanding the given data in Fourier series/spherical harmonic series, the problem (4.2), after a polar (in two dimensions) and spherical (in three dimensions) transform, reduces to a sequence of one-dimensional problems (for brevity, we use u to denote the Fourier/spherical harmonic expansion coefficients of U, and likewise, we use u_0, u_1, h, and f to denote the expansion coefficients of U_0, U_1, H, and F, respectively):

$$\begin{aligned}
&\frac{\partial^2 u}{\partial t^2} - \frac{c^2}{r^{d-1}}\frac{\partial}{\partial r}\left(r^{d-1}\frac{\partial u}{\partial r}\right) + c^2\beta_n\frac{u}{r^2} = f, \quad b_0<r<b,\ \ t>0;\\
&u|_{t=0} = u_0, \quad \frac{\partial u}{\partial t}\Big|_{t=0} = u_1, \quad b_0<r<b; \quad u|_{r=b_0} = 0,\ \ t>0;\\
&\left(\frac{1}{c}\frac{\partial u}{\partial t} + \frac{\partial u}{\partial r} + \frac{d-1}{2r}u\right)\Big|_{r=b} = \int_0^t \sigma_\nu(t-\tau)u(b,\tau)d\tau + h,\ \ t>0,
\end{aligned} \tag{4.3}$$

where $\beta_n = n^2, n(n+1)$ and $\nu = n, n+1/2$ for $d=2,3$, respectively. Since σ_ν is real, the real and imaginary parts of u and the given data can be decoupled. In what follows, we assume they are real.

4.3. Spectral-Galerkin approximation in space. We apply the Legendre spectral-Galerkin method to approximate (4.3) in space. For convenience of implementation, we transform the interval (b_0, b) into the reference interval $I=(-1,1)$ by $r = \frac{b-b_0}{2}x + \frac{b+b_0}{2}$ with $x\in\bar{I}$ and denote the transformed functions by $v(x,t) = u(r,t)$, $g(x,t) = f(r,t)$, and $v_i(x) = u_i(r)$ with $i=0,1$, respectively. Then (4.3) can be reformulated as

$$\begin{aligned}
&\frac{\partial^2 v}{\partial t^2} - \frac{\tilde{c}^2}{(x+c_0)^{d-1}}\frac{\partial}{\partial x}\left((x+c_0)^{d-1}\frac{\partial v}{\partial x}\right) + \tilde{c}^2\beta_n\frac{v}{(x+c_0)^2} = g, \quad x\in I,\ \ t>0;\\
&v(x,0) = v_0(x), \quad \frac{\partial v}{\partial t}(x,0) = v_1(x), \quad x\in I; \quad v(-1,t) = 0,\ \ t>0;\\
&\left(\frac{1}{c}\frac{\partial v}{\partial t} + \frac{2}{b-b_0}\frac{\partial v}{\partial x} + \frac{d-1}{2b}v\right)(1,t) = \int_0^t \sigma_\nu(t-\tau)v(1,\tau)d\tau + h(t),\ \ t>0,
\end{aligned} \tag{4.4}$$

where the constants $\tilde{c} = \frac{2c}{b-b_0}$ and $c_0 = \frac{b+b_0}{b-b_0}$.

Let $V_N := \big\{\psi\in P_N : \psi(-1) = 0\big\}$, where P_N is the set of all algebraic polynomials of degree at most N. The semidiscretization Legendre spectral-Galerkin approximation of (4.4) is to find $v_N(x,t)\in V_N$ for all $t>0$ such that for all $w\in V_N$,

$$\begin{aligned}
&(\ddot{v}_N, w)_\varpi + \tilde{c}(1+c_0)^{d-1}\dot{v}_N(1,t)w(1) + \tilde{c}^2(\partial_x v_N, \partial_x w)_\varpi + \tilde{c}^2\beta_n\big(v_N(x+c_0)^{-2}, w\big)_\varpi\\
&\qquad + \frac{2c^2}{b-b_0}(1+c_0)^{d-1}\left(\frac{d-1}{2b}v_N(1,t) - \sigma_\nu(t) * v_N(1,t)\right)w(1)\\
&\quad = (I_N g, w)_\varpi + \frac{2c^2}{b-b_0}(1+c_0)^{d-1}h(t)w(1), \quad t>0,\\
&v_N(x,0) = v_{0,N}(x), \quad \dot{v}_N(x,0) = v_{1,N}(x), \quad x\in I,
\end{aligned} \tag{4.5}$$

where $(\cdot,\cdot)_\varpi$ is the (weighted) inner product of $L^2_\varpi(I)$ with the weight function $\varpi = (x+c_0)^{d-1}$, $\ddot{v}$ denotes $\partial_t^2 v$ or $\frac{d^2v}{dt^2}$ as usual, I_N is the interpolation operator on $(N+1)$ Legendre–Gauss–Lobatto points, and $v_{0,N}, v_{1,N} \in P_N$ are suitable approximations of the initial values.

As in Theorem 3.5, we have the following a priori estimates.

THEOREM 4.1. *Let v_N be the solution of* (4.5). *If $h \in L^\infty(0,T)$, $\partial_t h \in L^1(0,T)$ and $g(\cdot,t) \in C(\bar{I})$. Then for all $T>0$,*

$$\begin{aligned}
&\|\partial_t v_N\|^2_{L^\infty(0,T;L^2_\varpi(I))} + \tilde{c}^2\big(\|\partial_x v_N\|^2_{L^\infty(0,T;L^2_\varpi(I))} + \beta_n\|v_N/(x+c_0)\|^2_{L^\infty(0,T;L^2_\varpi(I))}\big)\\
&\le C\big(\|v_{1,N}\|^2_{L^2_\varpi(I)} + \tilde{c}^2\big(\|\partial_x v_{0,N}\|^2_{L^2_\varpi(I)} + \beta_n\|v_{0,N}/(x+c_0)\|^2_{L^2_\varpi(I)}\big)\\
&\quad + \|h\|^2_{L^\infty(0,T)} + \|\partial_t h\|^2_{L^1(0,T)} + \|I_N g\|^2_{L^1(0,T;L^2_\varpi(I))}\big),
\end{aligned} \tag{4.6}$$

where C is a positive constant independent of N.

Proof. Taking $w = \partial_t v_N$ in (4.5) and integrating the resulting equation with respect to t, we use Corollary 3.4 and an argument similar to that for Theorem 3.5 to derive the estimates. ∎

REMARK 4.1. *Equipped with Theorem* 4.1*, we can analyze the convergence of the semidiscretized scheme* (4.5) *as on page* 341 *of* [42].

We next examine the linear system of (4.5). As shown in [41, 42], it is advantageous to construct basis functions satisfying the underlying homogeneous Dirichlet boundary conditions. Let $L_l(x)$ be the Legendre polynomial of degree l (see, e.g., [48]), and define

$$\begin{aligned}
&\phi_k(x) = L_k(x) + L_{k+1}(x),\\
&\Rightarrow\ \phi_k(-1) = 0 \ \text{ and } \ V_N = \operatorname{span}\{\phi_k : 0 \le k \le N-1\}.
\end{aligned} \tag{4.7}$$

Note that $\phi_k(1) = 2$. Setting

$$v_N(x,t) = \sum_{j=0}^{N-1} \hat{v}_j(t)\phi_j(x),\ \ \boldsymbol{v} = (\hat{v}_0, \hat{v}_1, \ldots, \hat{v}_{N-1})^t,\ \ m_{ij} = (\phi_j,\phi_i)_\varpi,\ \ s_{ij} = (\phi_j',\phi_i')_\varpi,$$

$$\tilde{m}_{ij} = \big(\phi_j(x+c_0)^{-2},\phi_i\big)_\varpi,\ \ \tilde{h}_i = (I_N g,\phi_i)_\varpi + \frac{c\alpha}{2}h,\ \ \boldsymbol{h} = (\tilde{h}_0,\tilde{h}_1,\ldots,\tilde{h}_{N-1})^t,$$

and $\mathbf{1} = (1,1,\ldots,1)^t$, we obtain the system

$$M\ddot{\boldsymbol{v}} + \alpha E\dot{\boldsymbol{v}} + \tilde{c}^2\big(S + \beta_n\widetilde{M}\big)\boldsymbol{v} + \mu E\boldsymbol{v} - c\alpha\left(\sigma_\nu * \sum_{j=0}^{N-1}\hat{v}_j\right)\mathbf{1} = \boldsymbol{h}, \tag{4.8}$$

with $\boldsymbol{v}(0) = \boldsymbol{v}_0$ and $\dot{\boldsymbol{v}}(0) = \boldsymbol{v}_1$, where $M = (m_{ij}), S = (s_{ij}), \widetilde{M} = (\tilde{m}_{ij})$, and $E = \mathbf{1}\mathbf{1}^t$ is an $N \times N$ matrix of all ones. In (4.8), $\boldsymbol{v}_0$ and $\boldsymbol{v}_1$ are column-N vectors of the expansion coefficients of $v_{0,N}$ and $v_{1,N}$ in terms of $\{\phi_k\}$, and the constants $\alpha = 8c(1+c_0)^{d-1}/(b-b_0)$ and $\mu = 4c^2(d-1)(1+c_0)^{d-1}/(b(b-b_0))$.

4.4. Newmark's time integration. To discretize the second-order ordinary differential system (4.8), we resort to the implicit second-order Newmark's scheme, which has wide applications in the field of structural mechanics (see [33, 53]). To this end, let Δt be the time-stepping size, let $\{\boldsymbol{v}^m, \dot{\boldsymbol{v}}^m, \ddot{\boldsymbol{v}}^m\}$ be the approximation of $\{\boldsymbol{v}, \dot{\boldsymbol{v}}, \ddot{\boldsymbol{v}}\}$ at $t = t_m = m\Delta t$, and let $\boldsymbol{h}^m = \boldsymbol{h}(t_m)$.

We first take care of the convolution term $\big[\sigma_\nu * \sum_{j=0}^{N-1}\hat{v}_j\big](t_{m+1})$ in (4.8):

$$
\begin{aligned}
&\left[\sigma_\nu * \sum_{j=0}^{N-1}\hat{v}_j\right](t_{m+1})\\
&= \sum_{j=0}^{N-1}\int_{t_m}^{t_{m+1}}\sigma_\nu(t_{m+1}-\tau)\hat{v}_j(\tau)d\tau + \sum_{j=0}^{N-1}\int_0^{t_m}\sigma_\nu(t_{m+1}-\tau)\hat{v}_j(\tau)d\tau \\
&\approx \frac{\Delta t}{2}\left(\sigma_\nu(0)\sum_{j=0}^{N-1}\hat{v}_j^{m+1} + \sigma_\nu(\Delta t)\sum_{j=0}^{N-1}\hat{v}_j^{m}\right) + \int_0^{t_m}\sigma_\nu(t_{m+1}-\tau)\left(\sum_{j=0}^{N-1}\hat{v}_j\right)(\tau)d\tau \\
&\approx \frac{\Delta t}{2}\sigma_\nu(0)E\boldsymbol{v}^{m+1} + \boldsymbol{g}^m,
\end{aligned}
\tag{4.9}
$$

where we used the Trapezoidal rule to approximate the integral over (t_m, t_{m+1}) and denoted by $\boldsymbol{g}^m$ the approximation of the remaining terms. Note that $\boldsymbol{g}^m$ depends on the history $\boldsymbol{v}^l (0 \le l \le m)$, but fortunately it can be evaluated recursively and rapidly as described in subsection 2.4. Moreover, only $\sum_{j=0}^{N-1}\hat{v}_j^m$ needs to be stored as an input for computing $\boldsymbol{v}^{m+1}$. As a result, the burden of the history dependence can be eliminated.

Denoting

$$
A = M,\ \ B = \alpha E,\ \ C = \tilde{c}^2\big(S + \beta_n\widetilde{M}\big) + \left(\mu - c\alpha\frac{\Delta t}{2}\sigma_\nu(0)\right)E,
\tag{4.10}
$$

and $\boldsymbol{f}^{m+1} = \boldsymbol{h}^{m+1} + c\alpha\boldsymbol{g}^m$, we carry out the full scheme for (4.4) as follows.

(i) Set $\boldsymbol{v}^0 = \boldsymbol{v}_0$ and $\dot{\boldsymbol{v}}^0 = \boldsymbol{v}_1$, and compute $\ddot{\boldsymbol{v}}^0$ from the system (4.8) by

$$
\ddot{\boldsymbol{v}}^0 = M^{-1}\big\{\boldsymbol{h}^0 - \alpha E\dot{\boldsymbol{v}}^0 - \tilde{c}^2\big(S + \beta_n\widetilde{M}\big)\boldsymbol{v}^0 - \mu E\boldsymbol{v}^0\big\},
\tag{4.11}
$$

where the convolution term vanishes at $t = 0$.

(ii) For $m \ge 0$, compute $\boldsymbol{v}^{m+1}$ from

$$
\begin{aligned}
\big(A + \vartheta\Delta t B + \theta\Delta t^2 C\big)\ddot{\boldsymbol{v}}^{m+1} = \boldsymbol{f}^{m+1} - B\big(\dot{\boldsymbol{v}}^m + (1-\vartheta)\Delta t\ddot{\boldsymbol{v}}^m\big)\\
- C\left(\boldsymbol{v}^m + \Delta t\dot{\boldsymbol{v}}^m + \frac{1-2\theta}{2}\Delta t^2\ddot{\boldsymbol{v}}^m\right),
\end{aligned}
\tag{4.12}
$$

and update $\boldsymbol{v}^{m+1}$ and $\dot{\boldsymbol{v}}^{m+1}$ by

$$
\boldsymbol{v}^{m+1} = \boldsymbol{v}^m + \Delta t\dot{\boldsymbol{v}}^m + \frac{1-2\theta}{2}\Delta t^2\ddot{\boldsymbol{v}}^m + \theta\Delta t^2\ddot{\boldsymbol{v}}^{m+1},
\tag{4.13}
$$

$$
\dot{\boldsymbol{v}}^{m+1} = \dot{\boldsymbol{v}}^m + (1-\vartheta)\Delta t\ddot{\boldsymbol{v}}^m + \vartheta\Delta t\ddot{\boldsymbol{v}}^{m+1},
\tag{4.14}
$$

respectively. It is known that in general, Newmark's scheme is of second order and unconditionally stable if the parameters satisfy $\vartheta \ge \frac{1}{2}$ and $\theta \ge \frac{1}{4}\big(\frac{1}{2}+\vartheta\big)^2$ (see, e.g., [53]).

4.5. Computational complexity. Let N_r and N_ϕ be the cutoff numbers in the radial and angular directions, respectively, and let N_t be the consecutive time steps. We approximate the solution of (4.2) by

$$
U_{\boldsymbol{N}}(r,\phi,t_m) = \sum_{|n|=0}^{N_\phi} u_{N_r,n}(r,t_m)e^{\mathrm{i}n\phi} \ \text{ or } \ U_{\boldsymbol{N}}(r,\theta,\phi,t_m) = \sum_{n=0}^{N_\phi}\sum_{|l|=0}^{n} u_{N_r,nl}(r,t_m)Y_n^l(\theta,\phi),
\tag{4.15}
$$

where $\boldsymbol{N} = (N_r, N_\phi)$, and $\{u_{N_r,n}, u_{N_r,nl}\}$ are computed from the proposed Legendre spectral-Galerkin and Newmark's scheme.

Some remarks on the complexity of the algorithm for (4.2) are in order.

(i) Discrete Fourier and spherical harmonic transforms are needed to assemble the solutions (in (4.15)) and transform the given data in (4.2) into the frequency space. It is known that the Fourier transform can be carried out by fast Fourier transform (FFT) with $O\big(N_\phi \log N_\phi\big)$ operations. The software SpherePack [47] can be used to perform the discrete spherical harmonic transform, though it is not optimal in computational complexity. However, substantial progress with $O\big(N_\phi^2 \log N_\phi\big)$ operations (cf. [46, 39]) has been made by using ideas stemming from the fast multipole method.

(ii) The coefficients $\{u_{N_r,n}, u_{N_r,nl}\}$ are computed from (4.12), so the major computational cost at each time step lies in inverting the coefficient matrix and evaluating the vectors on the right-hand side of (4.12).

(a) Notice that under the basis $\{\phi_k\}$ (cf. (4.7)), the matrices M and $\widetilde{M}$ (for $d = 3$ or $d = 2$ and $b_0 = 0$) are sparse with small bandwidth, and their entries can be evaluated exactly by using the properties of Legendre polynomials (cf. Chapter 4 of [42]). For $d = 2$ and $b_0 > 0$, one may take $\varpi = (x + c_0)^2$ in (4.5) (note: the "weight function" is bounded below away from 0), so that $\widetilde{M}$ will be tridiagonal. Although the matrices E and S in (4.10) are full, they can be converted to sparse matrices coincidentally by a simultaneous elimination. Let P be an $N_r \times N_r$ fundamental matrix for elementary row operations, whose entries on the main diagonal (resp., lower off-diagonal) are all 1 (resp., -1), and the other entries are 0. One finds $PEP^t = \mathrm{diag}(1, 0, \ldots, 0)$, and

$$(PS)_{ij} = s_{ij} - s_{i-1,j}, \quad (PSP^t)_{ij} = s_{ij} - s_{i,j-1} + s_{i-1,j-1} - s_{i-1,j},$$

where $(\,\cdot\,)_{ij}$ denotes the entry of the involved matrix, and we set $s_{ij} = 0$ if i or j is negative. By the definition of s_{ij}, we obtain from (4.7) that

$$\begin{aligned}(PSP^t)_{ij} &= \int_{-1}^{1} (\phi_i - \phi_{i-1})'(\phi_j - \phi_{j-1})'(x + c_0)^{d-1} dx \\ &= (2i+1)(2j+1) \int_{-1}^{1} L_i(x) L_j(x) (x + c_0)^{d-1} dx,\end{aligned} \tag{4.16}$$

where we used the property $(2k+1)L_k = L'_{k+1} - L'_{k-1}$ (cf. [42, eq. (3.176a)]). Then one verifies readily from the three-term recurrence relation and orthogonality of Legendre polynomials that PSP^t is tridiagonal for $d = 2$ and is pentadiagonal for $d = 3$. It is clear that the operations acting on the matrices M and $\widetilde{M}$, i.e., PMP^t and $P\widetilde{M}P^t$, increase only two more nonzero off-diagonals. In summary, with this simple preprocessing, the coefficient matrix of (4.12) becomes sparse with small bandwidth, which can be inverted efficiently with nearly $O(N_r)$ operations (cf. [42, Chapter 4]).

(b) As a typical spectral approximation using a modal basis, discrete Legendre transforms between the physical and frequency spaces are necessary for computing, e.g., $\boldsymbol{f}^{m+1}$, which can be done by matrix-vector multiplication in $O(N_r^2)$ operations (cf. [42]). Alpert and Rokhlin [4] developed an $O(N_r \log N_r)$ algorithm by evaluating Legendre coefficients and physical values on Chebyshev nodes, and Iserles [25] proposed a fast and simple algorithm with similar complexity for functions analytic in a sizable ellipse.

(c) We reiterate the overheads for evaluating the temporal convolution in (4.9). First, the zeros $\{z_j^\nu\}_{j=1}^{M_\nu}$ of $K_\nu(z)(\nu = n, n+1/2)$ must be precomputed to evaluate $\sigma_\nu(0)$ and $\sigma_\nu(\Delta t)$ in (4.9) and the temporal convolution. Note that the symmetry of the zeros (cf. Lemma 2.1) enables us to halve the computational cost if we use Newton's method with initial guess in [15]. Another practical algorithm (cf. [29]) could be used to find the zeros of $K_{n+1/2}(z)$ for any $n \le 1000$ accurately in negligible time, which can be extended to compute zeros of $K_n(z)$ easily. Second, armed with the zeros, the vector $\boldsymbol{g}^m$, computed by recurrence marching as in (2.30)–(2.31), requires $O(m)$ operators for the factor f in the sum and integral, so the cost for the convolution at $t = t_m$ in (2.31) is $O(mN_\phi)$ (note: $M_\nu \sim N_\phi$). Moreover, it is seen from (4.9) that we need only store the sum of Legendre coefficients at previous steps.

(iii) In a nutshell, the computational cost of the solver consists of the overheads for the Legendre spectral-Galerkin–Newmark scheme for each mode $\{u_{N_r,n}, u_{N_r,nl}\}$ and Fourier/spherical harmonic transforms:

$$\big\{\big[O(N_r^2) + O(N_\phi)\big] \times (2N_\phi + 1)\big\} \times N_t + O(N_\phi \log N_\phi) \quad \text{for } d = 2, \tag{4.17}$$

$$\big\{\big[O(N_r^2) + O(N_\phi)\big] \times (N_\phi + 1)^2\big\} \times N_t + O(N_\phi^2 \log N_\phi) \quad \text{for } d = 3, \tag{4.18}$$

where $O(N_t N_\phi)$ counts the contribution of computing the temporal convolution of each mode. As mentioned before, $O(N_r^2)$ for the Legendre transforms can be reduced to $O(N_r \log N_r)$ (cf. [4]), and with the matrix operations shown in (ii)(a), the system (4.12) can be solved in nearly $O(N_r)$ operations. It is important to point out that the modes $\{u_{N_r,n}, u_{N_r,nl}\}$ can be computed in parallel, as they are decoupled.

REMARK 4.2. *As outlined in subsection* 4.1*, the coupling with the TFE method for general scatterers requires a truncation of* (4.1)*, e.g., for* $d = 2$*, the numerical solution* $U_{\rm sol} = \sum_{l=0}^{N_\varepsilon} U_{l,\boldsymbol{N}} \varepsilon^l$ *for a given cut-off* N_ε*, where* $\{U_{l,\boldsymbol{N}}\}$ *are obtained from* (4.15) *by the solver. Hence, an* N_ε *multiple of the cost in* (4.17)–(4.18) *is expected.*

The spectral solver should be of optimal complexity (cf. [42, Chapter 8]). However, in this context, a higher price is paid for the temporal convolution, where the number of zeros (poles) grows linearly with N_ϕ. One idea to reduce the cost is to use the compressed rational approximation proposed in [2] to approximate σ_ν, which may result in a reduction to $O(N_t \log^2 N_\phi + N_t \log N_\phi \log \frac{1}{\varepsilon})$ for a prescribed accuracy threshold ε in the sense of [2].

Here, we describe a simple approach based on the observation that for slightly large t, the contribution of the zeros z_j^n far away from the imaginary axis to the value of σ_n is exponentially small, as $\min_j\{\mathrm{Re}(z_j^n)\} \sim -na$ (where $a \approx 0.66274$) for large order n. Moreover, the zeros are much denser near the left side of the eye-shaped curve (see Figure 2.1). Hence, we propose to modify the two-dimensional convolution kernel as $\tilde\sigma_n(t) = \sigma_n(t)$ for $0 \le t < t_0$ and

$$\tilde\sigma_n(t) = \frac{c}{b^2}\left\{\sum_{j\in\Upsilon_n^\delta} z_j^n e^{ctz_j^n/b} + (-1)^n \int_0^\infty \frac{e^{-ctr/b}}{K_n^2(r) + \pi^2 I_n^2(r)} dr\right\} \quad \forall\, t \ge t_0,\ \ n \gg 1, \tag{4.19}$$

where $\Upsilon_n^\delta = \{j : \mathrm{Re}(z_j^n) \ge -\delta(na)\}$ for some $\delta \in (0,1)$ (note: δ tunes the number of zeros used for the summation). Notice that the integral term can be computed via (2.25) in negligible time. Accordingly, we denote the modified DtN operator (cf. (2.7)) by $\widetilde{T}_d(U)$. We now examine the error induced by this approximation. If the

solution $U \in H_p^s(0, 2\pi)$ (in the ϕ direction and where p means the periodicity), it is known that the Fourier coefficients $\widehat{U}_n \sim n^{-s}$ for all t. Then we have

$$
\begin{aligned}
T_d(\widehat{U}_n) - \widetilde{T}_d(\widehat{U}_n) = (\sigma_n - \tilde{\sigma}_n) * \widehat{U}_n &= \frac{c}{b^2} \sum_{j \notin \Upsilon_n^\delta} z_j^n \int_{t_0}^t e^{c\tau z_j^n/b} \widehat{U}_n(b, t-\tau) d\tau \\
&\sim \frac{1}{bn^s} \sum_{j \notin \Upsilon_n^\delta} \left(e^{ctz_j^n/b} - e^{ct_0 z_j^n/b} \right) \sim \left(\sum_{j \notin \Upsilon_n^\delta} e^{ct_0 z_j^n/b} \right) n^{-s}.
\end{aligned} \tag{4.20}
$$

Roughly, the factor in the parentheses is dominated by $e^{-c\delta n a t_0/b}$. In practice we can choose $t_0 \sim (c\delta n a/b)^{-\epsilon}$ for some $0 < \epsilon < 1$ so that the factor will be uniformly bounded. The three-dimensional NRBK can be treated in a similar fashion. This allows us to significantly reduce the cost for computing temporal convolution without loss of accuracy. This will be further confirmed by the numerical results in the forthcoming section.

5. Numerical results. In this section, we present various numerical results to show the accuracy and convergence of the proposed algorithm, and to demonstrate the efficiency of the reduction by (4.19).

Typically, we test the algorithm by computing the waves scattered by a disk of radius $r = b_0$ and by the impedance data $G(\phi, t), \phi \in [0, 2\pi)$, and $t \geq 0$. It is known that this problem admits a series solution (see Appendix C for the derivation), which can be used as a reference solution to examine various aspects of the algorithm.

PROPOSITION 5.1. *The exterior problem* (2.1)–(2.3) *with* $d = 2$, $D = \{\boldsymbol{x} \in \mathbb{R}^2 : |\boldsymbol{x}| < b_0\}$, $F = U_0 = U_1 \equiv 0$, *and* $U|_{r=b_0} = G$ *admits the solution* $U(r, \phi, t) = \sum_{|n|=0}^{\infty} \widehat{U}_n(r, t) e^{\mathrm{i}n\phi}$ *for* $r > b_0$, $\phi \in [0, 2\pi)$, $t > 0$, *where*

$$
\widehat{U}_n(r, t) = \begin{cases} 0, & t < \beta_0, \\ H_n(r, t) * \widehat{G}_n(t - \beta_0) + \sqrt{b_0/r}\, \widehat{G}_n(t - \beta_0), & t \geq \beta_0, \end{cases} \tag{5.1}
$$

with $\beta_0 = (r - b_0)/c$, $\widehat{G}_n(t)$ *being the Fourier expansion coefficient of* $G(\phi, t)$, *and*

$$
\begin{aligned}
H_n = &\frac{c}{b_0} \sum_{j=1}^{M_n} \frac{K_n(rz_j^n/b_0)}{K_n'(z_j^n)} e^{tcz_j^n/b_0} \\
&+ (-1)^n \frac{c}{b_0} \int_0^\infty \frac{I_n(r\rho/b_0) K_n(\rho) - K_n(r\rho/b_0) I_n(\rho)}{K_n^2(\rho) + \pi^2 I_n^2(\rho)} e^{-ct\rho/b_0} d\rho,
\end{aligned}
$$

where $\{z_j^n\}$ *are zeros of* $K_n(z)$.

REMARK 5.1. *Similarly, the exact solution of the three-dimensional exterior problem can be obtained by using the same approach as in Appendix* C *but with the right contour in Figure* A.1.

5.1. Accuracy of the NRBCs. Our first task is to examine the accuracy of the NRBCs. For this purpose, we choose the "wave-maker" to be

$$
G(\phi, t) = A_1 e^{-\iota((b_0 \cos\phi - x_s)^2 + (b_0 \sin\phi - y_s)^2)} \sin^p(\omega t), \tag{5.2}
$$

with the parameters $A_1 = 10$, $\iota = 0.1$, $x_s = y_s = 2.1$, $b_0 = 2$, and ω, p are to be specified later. Its Fourier coefficients $\{\widehat{G}_n\}$ can be computed accurately via FFT.

The improper integral in (5.1) can be treated in a similar manner as the improper integral of $\sigma_n(t)$ in subsection 2.3.

Define the error of the NRBC for the problem in Proposition 5.1:

$$E_{N_\phi}(t) = \max_{|n|\le N_\phi} \left| \left(\frac{1}{c}\frac{\partial \widehat{U}_n}{\partial t} + \frac{\partial \widehat{U}_n}{\partial r} + \frac{\widehat{U}_n}{2r} \right)\Big|_{r=b} - \sigma_n(t) * \widehat{U}_n(b,t) \right|, \quad t>0, \tag{5.3}$$

where $\{\widehat{U}_n(b,t)\}$ are computed from (5.1), and we take $N_\phi = 32$ so that $\{|\widehat{U}_n(b,t)|\}$ are sufficiently small for all modes $|n| \le N_\phi$ and all t of interest.

We tabulate in Table 5.1 the errors with various parameters and time t, where we choose the radius b so that the reference solution $U_{N_\phi}(b,\phi,t) = \sum_{|n|=0}^{N_\phi} \widehat{U}_n(b,t)e^{in\phi}$ has a bigger magnitude. We see that in all cases, the errors are almost machine zero. This validates the formula for σ_n in Theorem 2.2 and shows the super-high accuracy of its numerical treatment.

TABLE 5.1
The errors $E_{N_\phi}(t)$.

t	$\omega = 10\pi$		$\omega = 20\pi$	
	$b = 2.22$	$b = 2.75$	$b = 2.38$	$b = 2.87$
0.5	2.637e-16	7.026e-17	6.245e-17	8.327e-17
1	4.684e-16	2.099e-16	9.021e-17	2.272e-16
5	2.567e-16	1.131e-15	7.251e-16	1.318e-15
10	7.772e-16	2.207e-15	1.457e-15	2.387e-15

As a comparison study, we demonstrate the accuracy of three different approaches for computing the NRBK σ_ν, i.e., the accurate formula in (2.20), the modified formula in (4.19), and the compressed rational approximation in [2]. Here, we extract the available data (for spherical kernel with 10^{-6} accuracy in [2]) from Hagstrom's website (http://faculty.smu.edu/thagstrom/sph6.txt). The intention is to compare their performance for large mode n. Hence, we choose the spherical harmonic expansion coefficient of the data at the scatterer's surface, which generates the three-dimensional exact solution (cf. Proposition 5.1 and Remark 5.1) to be $\sin^6(\pi t)$. In Table 5.2, we list the accuracy measured as in (5.3), but for $d = 3$ and each fixed mode. We see that the use of a comparable number of zeros (compressed poles in [2]) leads to a very similar accuracy. We reiterate that the simple modified approach in (4.19) requires us to use all zeros for $0 \le t < t_0$.

TABLE 5.2
Comparison of three approaches ($t = 3.5$, $t_0 = 0.2$, $b = 2.1$, $c = 5$).

n	Approach by (2.20)		Approach by (4.19)		Approach in [2]	
(Total zeros)	Accuracy	Used zeros	Accuracy	Used zeros	Accuracy	Used poles
60	1.3223e-12	60	1.6646e-07	10	1.6763e-07	11
70	1.7082e-12	70	4.2907e-08	12	2.6160e-07	11
90	2.6909e-12	90	1.1889e-09	12	6.8482e-08	12
100	7.5346e-12	100	2.6676e-09	12	6.9170e-08	12

5.2. Convergence of the algorithm for smooth solutions. The second task is to demonstrate the accuracy and convergence of the spectral-Galerkin–Newmark scheme described in section 4. Let $\{u_{N_r,n}(r,t_m)\}$ be the numerical solutions (as defined in (4.15)) computed by the scheme, which approximate the corresponding reference solutions $\{\widehat{U}_n(r,t_m)\}$ in Proposition 5.1. Here, we take N_ϕ so that the magnitudes of the truncated modes $\{|\widehat{U}_n|\}_{|n|>N_\phi}$ are sufficiently small, and the parameters

are taken as before. The numerical errors are measured by

$$\widehat{E}_{\boldsymbol{N}}(t) = \max_{|n|\le N_\phi} \left\| u_{N_r,n}(\cdot,t) - \widehat{U}_n(\cdot,t) \right\|_{L^2,N_r},$$

$$\widetilde{E}_{\boldsymbol{N}}(t) = \max_{|n|\le N_\phi} \left\| u_{N_r,n}(\cdot,t) - \widehat{U}_n(\cdot,t) \right\|_{L^\infty,N_r},$$

where $\boldsymbol{N} = (N_r, N_\phi)$, $\|\cdot\|_{L^2,N_r}$ is the discrete L^2-norm associated with the Legendre–Gauss–Lobatto points, and $\|\cdot\|_{L^\infty,N_r}$ is the corresponding discrete maximum norm.

We list in Table 5.3 the errors and convergence order in time discretization, where we choose $N_r = 50, N_\phi = 15$ so that the error of spatial discretization is negligible, and the other parameters are $b = 5$, $\omega = \pi$, and $p = 6$. As expected, we observe a second-order convergence of Newmark's scheme.

To see the spectral accuracy of the Legendre–Galerkin approximation, we take $\Delta t = 10^{-5}$ and fix other parameters but vary N_r. Observe from Table 5.4 a fast decay of the errors as a typical spectral approximation, which also shows that the scheme is quite stable.

TABLE 5.3
The errors $\widehat{E}_{\boldsymbol{N}}(t)$ and $\widetilde{E}_{\boldsymbol{N}}(t)$, and order of convergence in time.

t	Δt	$\widehat{E}_{\boldsymbol{N}}(t)$	Order	$\widetilde{E}_{\boldsymbol{N}}(t)$	Order
1	1e-3	1.21e-5		1.93e-5	
	5e-4	3.02e-6	2.00005	4.83e-6	1.99994
	1e-4	1.21e-7	1.99993	1.93e-7	1.99986
	5e-5	3.02e-8	2.00012	4.83e-8	1.99906
2	1e-3	1.23e-5		2.01e-5	
	5e-4	3.07e-6	1.99998	5.02e-6	1.99997
	1e-4	1.23e-7	2.00001	2.01e-7	1.99998
	5e-5	3.07e-8	2.00002	5.02e-8	1.99993
3	1e-3	1.23e-5		2.01e-5	
	5e-4	3.07e-6	2.00007	5.02e-6	1.99997
	1e-4	1.23e-7	1.99997	2.01e-7	1.99998
	5e-5	3.07e-8	2.00007	5.02e-8	2.00004
4	1e-3	1.23e-5		2.01e-5	
	5e-4	3.07e-6	2.00007	5.02e-6	1.99997
	1e-4	1.23e-7	1.99997	2.01e-7	1.99998
	5e-5	3.07e-8	2.00007	5.02e-8	2.00004

TABLE 5.4
The errors $\widehat{E}_{\boldsymbol{N}}(t)$ and $\widetilde{E}_{\boldsymbol{N}}(t)$.

t	$N_r = 8$		$N_r = 10$		$N_r = 16$		$N_r = 32$	
	$\widehat{E}_{\boldsymbol{N}}(t)$	$\widetilde{E}_{\boldsymbol{N}}(t)$	$\widehat{E}_{\boldsymbol{N}}(t)$	$\widetilde{E}_{\boldsymbol{N}}(t)$	$\widehat{E}_{\boldsymbol{N}}(t)$	$\widetilde{E}_{\boldsymbol{N}}(t)$	$\widehat{E}_{\boldsymbol{N}}(t)$	$\widetilde{E}_{\boldsymbol{N}}(t)$
2.0	4.105e-4	4.368e-4	1.092e-5	1.188e-5	7.353e-9	1.238e-8	1.237e-9	2.119e-9
2.5	3.239e-4	3.607e-4	5.724e-6	6.997e-6	2.381e-9	3.182e-9	1.488e-9	1.734e-9
3.0	4.113e-4	4.380e-4	1.095e-5	1.189e-5	1.404e-9	2.893e-9	1.227e-9	2.009e-9
3.5	3.238e-4	3.608e-4	5.747e-6	7.036e-6	1.554e-9	2.063e-9	1.488e-9	1.732e-9
4.0	4.113e-4	4.380e-4	1.095e-5	1.189e-5	1.269e-9	2.061e-9	1.227e-9	2.007e-9

Finally, we plot in Figure 5.1 the numerical solution (red nets) against the exact solution (blue smooth surface), where the exact solution in (a) and (b) is in the annulus $2 \le r \le 10$, while the numerical solution is within $2 \le r \le 5$. Figure 5.1(c) shows the wave propagation through the artificial boundary at $b = 5, 0 \le \phi \le 2\pi$ for $0 \le t \le 4$ (numerical solution) against $0 \le t \le 4.5$ (exact solution). We see that the red nets and blue surfaces agree well in these plots. Moreover, we observe that the waves pass the boundary transparently. This shows that the proposed scheme is very stable and accurate.

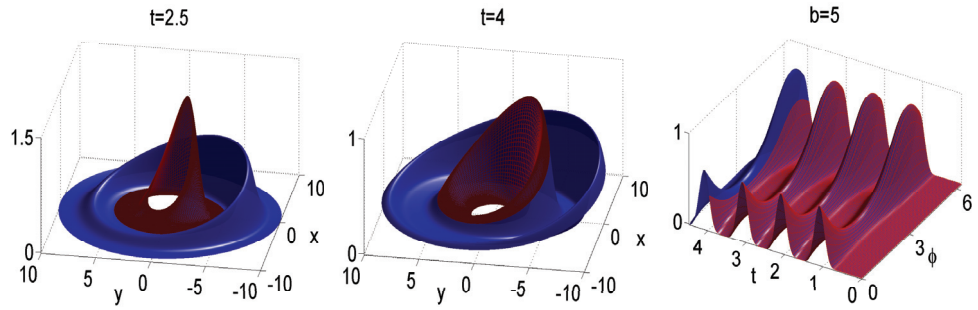

(a) (b) (c)

FIG. 5.1. *Propagation of exact and numerical solutions.*

5.3. Test for the modification of NRBCs. To illustrate the effectiveness of the modification in (4.19)–(4.20), we take the Dirichlet data G to be less regular in the ϕ-direction:

$$G = y^{\lambda} e^{xy/2} \sin^6(\pi t) = e^{b_0^2 \cos\phi \sin\phi/2} (b_0 \sin\phi)^{\lambda} \sin^6(\pi t), \tag{5.4}$$

where $\lambda > 0$ is a noninteger constant. One verifies that $G \in H_p^{\lambda+1/2-\varepsilon}(0, 2\pi)$ (for small $\varepsilon > 0$) and its Fourier coefficients decay like $O(N_\phi^{\varepsilon-(\lambda+1/2)})$. The Fourier coefficients of the exact solution in Proposition 5.1 are expected to decay in a similar fashion.

Hereafter, we take $\lambda = 2.5, b_0 = 2, b = c = 3$ and use the modified NBRK $\tilde{\sigma}_n$ in (4.19) for $n \geq 20$, and $t \geq t_0 = (c\delta na/b)^{-\epsilon}$ (cf. (4.20); note that $a = 0.66274$) with $\epsilon = 0.9$. Recall that the poles $\{z_j^n\}$ are dropped if $\mathrm{Re}(z_j^n) < -\delta na$. As $\{z_j^n\}$ are very dense on the left portion of the eye-shaped curve (cf. Figure 2.1), many poles can be dropped (about 90%, as shown in Table 5.5) for large n and all $t \geq t_0$. Moreover, equipped with the guideline in (4.19)–(4.20), such a modification does not deteriorate the accuracy and stability of the algorithm, as shown in Figure 5.2.

TABLE 5.5
The number of used poles and the starting time of modification.

n	$\delta = 0.4$			$\delta = 0.5$		
	Used	Total	t_0	Used	Total	t_0
55	6	54	0.090	10	54	0.073
65	8	64	0.077	10	64	0.063
75	8	74	0.068	12	74	0.055
90	10	90	0.058	16	90	0.047
100	12	100	0.052	18	100	0.043
110	12	110	0.048	18	110	0.039

5.4. Test for three-dimensional case. Now, we examine the performance of the proposed algorithm for the three-dimensional case. In the following test, we take

$$G(\theta, \phi, t) = 50\big[1 - \tanh(2\cos\phi \sin(5\theta))\big] \sin^6(\pi t) \tag{5.5}$$

and choose $b_0 = 2, b = c = 3$. The reference exact solution (cf. Remark 5.1) is evaluated by a very fine mesh, and the numerical solution is computed by the spherical harmonic expansion (4.15), where the coefficients are computed by the one-dimensional solver (4.5). We tabulate in Table 5.6 the (discrete) L^2-errors with $N_r = 30, N_\phi = 100$, and

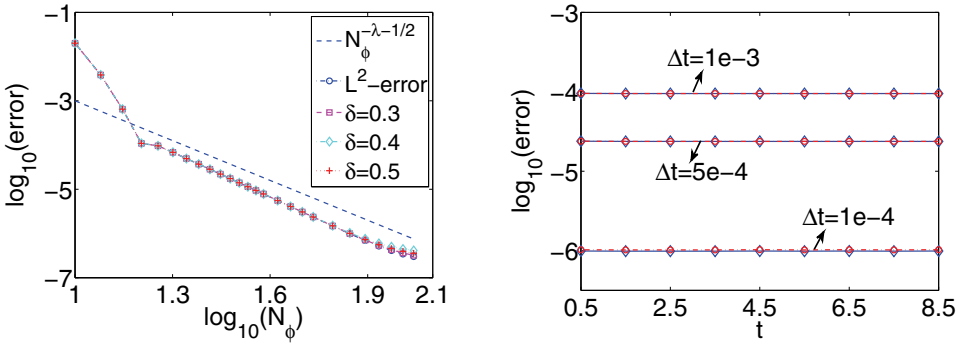

FIG. 5.2. *Left:* $\log_{10}(L^2\text{-error})$ *against* $\log_{10}(N_\phi)$ *with* $N_r = 30$ *and* $\Delta t = 5e-5$ *at* $t = 2.5$. *Right: stability "without modification" (marked by "–◇") and "with modification" (marked by "–.○"), where* $N_\phi = 100, N_r = 30$, *and* $\delta = 0.4$.

TABLE 5.6
Second-order convergence in time.

t	Δt	Error	Order	t	Δt	Error	Order
1	1e-3	3.61e-5		2	1e-3	3.53e-5	
	5e-4	9.04e-6	2.00		5e-4	8.81e-6	2.00
	1e-4	3.61e-7	2.00		1e-4	3.53e-7	2.00
	5e-5	9.04e-8	1.99		5e-5	8.81e-8	1.99
3	1e-3	3.52e-5		4	1e-3	3.52e-5	
	5e-4	8.81e-6	2.00		5e-4	8.81e-6	2.00
	1e-4	3.52e-7	2.00		1e-4	3.52e-7	2.00
	5e-5	8.81e-8	2.00		5e-5	8.81e-8	2.00

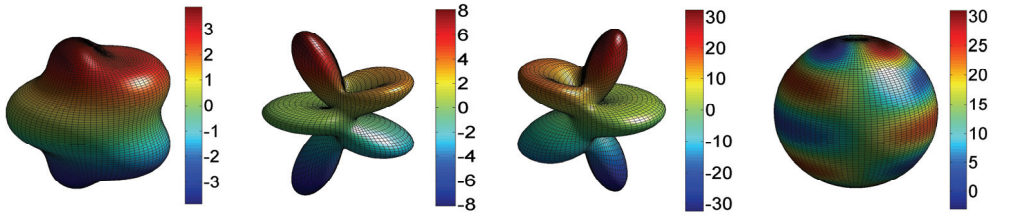

(a) $t = 0.5$. (b) $t = 1.5$. (c) $t = 2$. (d) $t = 2$.

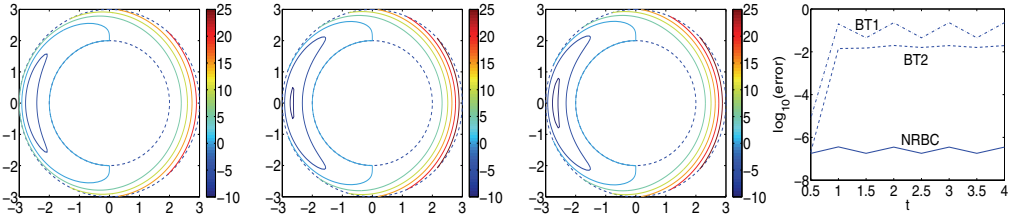

(e) BT1. (f) BT2. (g) NRBC. (h) Convergence.

FIG. 5.3. *Numerical solution at different time* t *at* $r = b$: (a)–(c) *function plot on the outer spherical surface;* (d) *surf-plot on spherical coordinates. Contour of numerical solution at* $t = 2$ *sliced by* $\theta = 15\pi/199$: (e)–(g) *BT1, BT2, NRBC.* (h) L^2*-errors obtained by three boundary conditions and the full algorithm with* $\Delta t = 10^{-4}, N_r = 30$, *and* $N_\phi = 100$.

various time step sizes Δt at different time t, which indicates a convergence behavior similar to the two-dimensional case (cf. Table 5.3). We depict in Figure 5.3(a)–(d) spherical plots of the waves on the artificial spherical boundary $r = b$, across which the outgoing waves propagate seamlessly.

Finally, we compare the convergence and accuracy of the algorithm using exact NRBCs and the low-order boundary conditions in [5] at $r = b$:

$$\text{(5.6)}\quad \text{BT1}:\quad \left(\frac{\partial}{\partial r}+\frac{\partial}{\partial t}\right)[ru]=0;\quad \text{BT2}:\quad \left(\frac{\partial}{\partial r}+\frac{\partial}{\partial t}\right)\left(\frac{\partial}{\partial r}+\frac{\partial}{\partial t}+\frac{2}{r}\right)[ru]=0.$$

We plot in Figure 5.3(e)–(g) the contour of the numerical solution sliced in θ, and in Figure 5.3(h) the convergence of the boundary conditions. We see that the NRBC produces a very accurate numerical solution, while BT1 and BT2 give very poor results.

Appendix A. Proof of Theorem 2.2. We first consider $d = 2$. Note that $F_n(z)$ is a multivalued function with branch points at $z = 0$ and infinity. The contour L for (2.15) is depicted in Figure A.1 (left) with the branch-cut along the negative real axis.

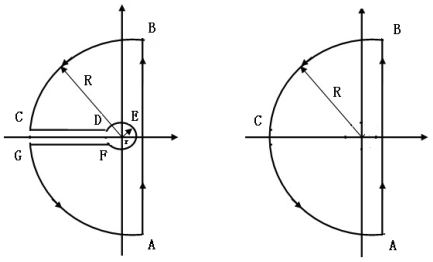

FIG. A.1. *Contour L for the inverse Laplace transform. Left: $d = 2$. Right: $d = 3$.*

We know from Lemma 2.1 that $F_n(z)$ has a finite number of simple poles in the second and third quadrants. Therefore, for any $n \geq 0$, it follows from the residue theorem that

$$\begin{aligned}\lim_{\substack{R\to+\infty\\ r\to 0^+}}\oint_L F_n(z)e^{czt/b}dz &= 2\pi\mathrm{i}\sum_{j=1}^{M_n}\mathrm{Res}\left[F_n(z)e^{czt/b},z_j^n\right]\\ &= 2\pi\mathrm{i}\sum_{j=1}^{M_n}\lim_{z\to z_j^n}\left\{(z-z_j^n)e^{czt/b}\left[z+\frac{1}{2}+z\frac{K_n'(z)}{K_n(z)}\right]\right\}=2\pi\mathrm{i}\sum_{j=1}^{M_n}e^{ctz_j^n/b}z_j^n.\end{aligned}\tag{A.1}$$

Thus, by (2.15) and (A.1),

$$\begin{aligned}\frac{2b^2\pi\mathrm{i}}{c}\sigma_n(t) &= 2\pi\mathrm{i}\sum_{j=1}^{M_n}e^{ctz_j^n/b}z_j^n-\lim_{\substack{R\to+\infty\\ r\to 0^+}}\left[\int_{\widehat{BC}}F_n(z)e^{czt/b}dz+\int_{\overline{CD}}F_n(z)e^{czt/b}dz\right.\\ &\quad\left.+\int_{\widehat{DEF}}F_n(z)e^{czt/b}dz+\int_{\overline{FG}}F_n(z)e^{czt/b}dz+\int_{\widehat{GA}}F_n(z)e^{czt/b}dz\right].\end{aligned}\tag{A.2}$$

In view of (2.14), we find from Jordan's lemma (cf. [16, 12]) and a direct calculation that

$$\lim_{\substack{R\to+\infty\\ r\to 0^+}}\left[\int_{\widehat{BC}}F_n(z)e^{czt/b}dz+\int_{\widehat{DEF}}F_n(z)e^{czt/b}dz+\int_{\widehat{GA}}F_n(z)e^{czt/b}dz\right]=0,\tag{A.3}$$

since each contour integral tends to zero. Thus, we only need to evaluate the integrals along the line segments $\overline{CD}$ and $\overline{FG}$. We have

$$\lim_{\substack{R\to+\infty\\ r\to 0^+}} \left[\int_{\overline{CD}} F_n(z)e^{czt/b}dz + \int_{\overline{FG}} F_n(z)e^{czt/b}dz\right] = \int_0^\infty re^{-ctr/b}\left[\frac{K_n'(re^{-\mathrm{i}\pi})}{K_n(re^{-\mathrm{i}\pi})} - \frac{K_n'(re^{\mathrm{i}\pi})}{K_n(re^{\mathrm{i}\pi})}\right]dr.$$

By Formula 9.6.31 of [1],

$$K_n(re^{\pi\mathrm{i}}) = e^{-n\pi\mathrm{i}}K_n(r) - \pi\mathrm{i}I_n(r), \quad K_n(re^{-\pi\mathrm{i}}) = e^{n\pi\mathrm{i}}K_n(r) + \pi\mathrm{i}I_n(r),$$

which, together with (2.13), implies

$$\begin{aligned}\frac{K_n'(re^{\mathrm{i}\pi})}{K_n(re^{\mathrm{i}\pi})} - \frac{K_n'(re^{-\mathrm{i}\pi})}{K_n(re^{-\mathrm{i}\pi})} &= \frac{K_{n+1}(re^{-\mathrm{i}\pi})}{K_n(re^{-\mathrm{i}\pi})} - \frac{K_{n+1}(re^{\mathrm{i}\pi})}{K_n(re^{\mathrm{i}\pi})}\\ &= \frac{e^{(n+1)\pi\mathrm{i}}K_{n+1}(r) + \pi\mathrm{i}I_{n+1}(r)}{e^{n\pi\mathrm{i}}K_n(r) + \pi\mathrm{i}I_n(r)} - \frac{e^{-(n+1)\pi\mathrm{i}}K_{n+1}(r) - \pi\mathrm{i}I_{n+1}(r)}{e^{-n\pi\mathrm{i}}K_n(r) - \pi\mathrm{i}I_n(r)}\\ &= \frac{(-1)^n 2\pi\mathrm{i}[K_{n+1}(r)I_n(r) + K_n(r)I_{n+1}(r)]}{K_n^2(r) + \pi^2 I_n^2(r)} = \frac{(-1)^n 2\pi\mathrm{i}}{r\big[K_n^2(r) + \pi^2 I_n^2(r)\big]},\end{aligned} \tag{A.4}$$

where we used the Wronskian identity (see Formula 9.6.15 of [1]):

$$I_n(z)K_{n+1}(z) + I_{n+1}(z)K_n(z) = z^{-1}. \tag{A.5}$$

A combination of (A.1)–(A.4) leads to

$$\sigma_n(t) = \frac{c}{b^2}\left\{\sum_{j=1}^{M_n} z_j^n e^{ctz_j^n/b} + \int_0^\infty \frac{(-1)^n e^{-ctr/b}}{K_n^2(r) + \pi^2 I_n^2(r)}dr\right\}, \tag{A.6}$$

which is the expression (2.19).

Now, we turn to the three-dimensional case. It is important to notice that the kernel function $F_{n+1/2}(z)$ is not a multivalued complex function, as opposed to the two-dimensional case. Indeed, although $K_{n+1/2}(z)$ is multivalued, in view of the formula (see page 80 of [52]),

$$K_{n+1/2}(z) = \sqrt{\frac{\pi}{2z}}\sum_{k=0}^{n}\frac{(n+k)!e^{-z}}{k!(n-k)!(2z)^k} \quad \forall n \ge 0, \tag{A.7}$$

the fact that $1/\sqrt{z}$ can be eliminated from the ratio $K_{n+1/2}'/K_{n+1/2}$. Thanks to this property, we use the contour in Figure A.1 (right), and by the residue theorem and Jordan's lemma, we have

$$\begin{aligned}\lim_{R\to+\infty}\oint_L F_{n+1/2}(z)e^{czt/b}dz &= \int_{\gamma-\infty\mathrm{i}}^{\gamma+\infty\mathrm{i}} F_{n+1/2}(z)e^{czt/b}dz\\ &= 2\pi\mathrm{i}\sum_{j=1}^{M_\nu}\mathrm{Res}\left[F_{n+1/2}(z)e^{czt/b}, z_j^\nu\right] = 2\pi\mathrm{i}\sum_{j=1}^{M_\nu} e^{ctz_j^\nu/b}z_j^\nu\end{aligned} \tag{A.8}$$

for $\nu = n + 1/2$. This leads to the formula (2.20).

Appendix B. Justification for Remark 2.2. Thanks to (2.17), we have

$$z\frac{H_\nu^{(1)'}(z)}{H_\nu^{(1)}(z)} = -\mathrm{i}z\frac{K_\nu'(-\mathrm{i}z)}{K_\nu(-\mathrm{i}z)}.$$

Thus, by (2.21) with $\nu = n$ and $-\mathrm{i}z = bs/c$, we find

$$\frac{s}{c} + \frac{1}{2b} + \frac{s}{c}\frac{K_n'(bs/c)}{K_n(bs/c)} = -\frac{\mathrm{i}c}{b^2}\sum_{j=1}^{N_n}\frac{h_{n,j}}{s+\frac{\mathrm{i}ch_{n,j}}{b}} + \frac{c}{b^2}\int_0^\infty \frac{(-1)^n}{K_n^2(r)+\pi^2 I_n^2(r)}\frac{1}{\frac{cr}{b}+s}dr.$$

Applying the inverse Laplace transform to both sides of the above identity leads to

$$\mathcal{L}^{-1}\left[\frac{s}{c} + \frac{1}{2b} + \frac{s}{c}\frac{K_n'(bs/c)}{K_n(bs/c)}\right] = \frac{c}{b^2}\sum_{j=1}^{N_n}(-\mathrm{i}h_{n,j})e^{-\mathrm{i}cth_{n,j}/b} + \frac{c}{b^2}\int_0^\infty \frac{(-1)^n e^{-crt/b}}{K_n^2(r)+\pi^2 I_n^2(r)}dr,$$

which turns out to be (A.6), since $-\mathrm{i}h_{n,j}$ are zeros of $K_n(z)$ and $N_n = M_n$. ∎

Appendix C. Proof of Proposition 5.1. This problem can be solved by Laplace transform and separation of variables. Indeed, the Fourier coefficients $\{\widehat{U}_n\}$ in (5.1) can be expressed as

$$\widehat{U}_n(r,t) = \mathcal{L}^{-1}\left(\frac{K_n(sr/c)}{K_n(sb_0/c)}\right)(t) * \widehat{G}_n(t), \quad r > b_0. \tag{C.1}$$

We next sketch the evaluation of the inverse Laplace transform by using the residue theorem as in Appendix A for $\sigma_n(t)$. Using (2.12), we find $\frac{K_n(sr/c)}{K_n(sb_0/c)} \sim \sqrt{\frac{b_0}{r}}e^{-s\beta_0}$, where $\beta_0 = (r-b_0)/c$. In order to use Jordan's lemma (cf. [16, 12]), we write

$$\begin{aligned}\mathcal{L}^{-1}\left(\frac{K_n(sr/c)}{K_n(sb_0/c)}\right)(t) &= \mathcal{L}^{-1}\left(e^{-\beta_0 s}\left\{e^{\beta_0 s}\frac{K_n(sr/c)}{K_n(sb_0/c)} - \sqrt{\frac{b_0}{r}}\right\}\right) + \mathcal{L}^{-1}\left(e^{-\beta_0 s}\sqrt{\frac{b_0}{r}}\right)(t)\\ &= \widetilde{H}_n(r,t-\beta_0)U_{\beta_0}(t) + \sqrt{\frac{b_0}{r}}\delta(t-\beta_0),\end{aligned} \tag{C.2}$$

where $\widetilde{H}_n(r,t) = \mathcal{L}^{-1}\big(e^{\beta_0 s}\frac{K_n(sr/c)}{K_n(sb_0/c)} - \sqrt{b_0/r}\big)(t)$, $U_{\beta_0}(t)$ is the unit step function (which takes 1 for $t \ge \beta_0$ and 0 for $t < \beta_0$), and $\delta(t)$ is the Dirac delta function. By applying the residue theorem and Jordan's lemma to the Bromwich's contour integral,

$$\widetilde{H}_n(r,t) = \frac{1}{2\pi\mathrm{i}}\int_{\gamma-\infty\mathrm{i}}^{\gamma+\infty\mathrm{i}}\left(e^{\beta_0 s}\frac{K_n(sr/c)}{K_n(sb_0/c)} - \sqrt{\frac{b_0}{r}}\right)e^{ts}ds, \tag{C.3}$$

we obtain (5.1) by using the contour in Figure A.1 (left) and the argument in Appendix A. Denoting $H_n(r,t) := \widetilde{H}_n(r,t-\beta_0)$, the desired expression follows from (C.2). ∎

Acknowledgments. The authors would like to thank the anonymous referees for many thoughtful comments, which were invaluable to the improvement of this paper. B. Wang would like to thank the Division of Mathematical Sciences of Nanyang Technological University for the hospitality during the visit.

REFERENCES

[1] M. Abramowitz and I. A. Stegun, eds., *Handbook of Mathematical Functions with Formulas, Graphs, and Mathematical Tables*, John Wiley & Sons, New York, 1984.

[2] B. Alpert, L. Greengard, and T. Hagstrom, *Rapid evaluation of nonreflecting boundary kernels for time-domain wave propagation*, SIAM J. Numer. Anal., 37 (2000), pp. 1138–1164.

[3] B. Alpert, L. Greengard, and T. Hagstrom, *Nonreflecting boundary conditions for the time-dependent wave equation*, J. Comput. Phys., 180 (2002), pp. 270–296.

[4] B. K. Alpert and V. Rokhlin, *A fast algorithm for the evaluation of Legendre expansions*, SIAM J. Sci. Stat. Comput., 12 (1991), pp. 158–179.

[5] A. Bayliss and E. Turkel, *Radiation boundary conditions for wave-like equations*, Comm. Pure Appl. Math., 33 (1980), pp. 707–725.

[6] J. P. Berenger, *A perfectly matched layer for the absorption of electromagnetic waves*, J. Comput. Phys., 114 (1994), pp. 185–200.

[7] S. C. Brenner and L. R. Scott, *The Mathematical Theory of Finite Element Methods*, 3rd ed., Texts Appl. Math. 15, Springer, New York, 2008.

[8] O. P. Bruno and F. Reitich, *Solution of a boundary value problem for the Helmholtz equation via variation of the boundary into the complex domain*, Proc. Roy. Soc. Edinburgh Sect. A, 122 (1992), pp. 317–340.

[9] Z. M. Chen, *Convergence of the time-domain perfectly matched layer method for acoustic scattering problems*, Int. J. Numer. Anal. Model., 6 (2009), pp. 124–146.

[10] P. G. Ciarlet, *The Finite Element Method for Elliptic Problems*, North–Holland, Amsterdam, 1978.

[11] R. D. Ciskowski and C. A. Brebbia, *Boundary Element Methods in Acoutics*, Kluwer Academic Publishers, Dordrecht, The Netherlands, 1991.

[12] A. M. Cohen, *Numerical Methods for Laplace Transform Inversion*, Numer. Methods Algorithms 5, Springer, New York, 2007.

[13] G. C. Cohen, *Higher-Order Numerical Methods for Transient Wave Equations*, Sci. Comput., Springer-Verlag, Berlin, 2002.

[14] M. D. Collins and W. A. Kuperman, *Inverse problems in ocean acoustics*, Inverse Problems, 10 (1994), pp. 1023–1040.

[15] A. Cruz and J. Sesma, *Zeros of the Hankel function of real order and of its derivative*, Math. Comp., 39 (1982), pp. 639–645.

[16] B. Davies, *Integral Transforms and Their Applications*, 3rd ed., Texts Appl. Math. 41, Springer-Verlag, New York, 2002.

[17] B. Engquist and A. Majda, *Absorbing boundary conditions for the numerical simulation of waves*, Math. Comp., 31 (1977), pp. 629–651.

[18] Q. R. Fang, D. P. Nicholls, and J. Shen, *A stable, high-order method for three-dimensional, bounded-obstacle, acoustic scattering*, J. Comput. Phys., 224 (2007), pp. 1145–1169.

[19] K. Gerdes and L. Demkowicz, *Solution of 3D-Laplace and Helmholtz equations in exterior domains using hp-infinite elements*, Comput. Methods Appl. Mech. Engrg., 137 (1996), pp. 239–273.

[20] D. Givoli, *Numerical Methods for Problems in Infinite Domains*, Stud. Appl. Mech. 33, Elsevier, Amsterdam, 1992.

[21] D. Givoli, *High-order local non-reflecting boundary conditions: A review. New computational methods for wave propagation*, Wave Motion, 39 (2004), pp. 319–326.

[22] M. J. Grote and J. B. Keller, *Exact nonreflecting boundary conditions for the time-dependent wave equation*, SIAM J. Appl. Math., 55 (1995), pp. 280–297.

[23] T. Hagstrom, *Radiation boundary conditions for the numerical simulation of waves*, Acta Numer., 8 (1999), pp. 47–106.

[24] R. N. Huan and L. L. Thompson, *Accurate radiation boundary conditions for the time-dependent wave equation on unbounded domains*, Internat. J. Numer. Methods Engrg., 47 (2000), pp. 1569–1603.

[25] A. Iserles, *A fast and simple algorithm for the computation of Legendre coefficients*, Numer. Math., 117 (2011), pp. 529–553.

[26] S. D. Jiang and L. Greengard, *Fast evaluation of nonreflecting boundary conditions for the Schrödinger equation in one dimension*, Comput. Math. Appl., 47 (2004), pp. 955–966.

[27] S. D. Jiang and L. Greengard, *Efficient representation of nonreflecting boundary conditions for the time-dependent Schrödinger equation in two dimensions*, Comm. Pure Appl. Math., 61 (2008), pp. 261–288.

[28] J. B. Keller and D. Givoli, *Exact nonreflecting boundary conditions*, J. Comput. Phys., 82 (1989), pp. 172–192.
[29] J. R. Li, *Low order approximation of the spherical nonreflecting boundary kernel for the wave equation*, Linear Algebra Appl., 415 (2006), pp. 455–468.
[30] C. Lubich and A. Schädle, *Fast convolution for nonreflecting boundary conditions*, SIAM J. Sci. Comput., 24 (2002), pp. 161–182.
[31] P. A. Martin, *Multiple Scattering: Interaction of Time-Harmonic Waves with N Obstacles*, Encyclopedia Math. Appl. 107, Cambridge University Press, Cambridge, UK, 2006.
[32] J. C. Nédélec, *Acoustic and Electromagnetic Equations. Integral Representations for Harmonic Problems*, Appl. Math. Sci. 144, Springer-Verlag, New York, 2001.
[33] N. M. Newmark, *A method of computation for structural dynamics*, J. Engrg. Mech. Div., 85 (1959), pp. 67–94.
[34] D. Nicholls and F. Reitich, *Analytic continuation of Dirichlet-Neumann operators*, Numer. Math., 94 (2003), pp. 107–146.
[35] D. P. Nicholls and J. Shen, *A stable high-order method for two-dimensional bounded-obstacle scattering*, SIAM J. Sci. Comput., 28 (2006), pp. 1398–1419.
[36] D. P. Nicholls and J. Shen, *A rigorous numerical analysis of the transformed field expansion method*, SIAM J. Numer. Anal., 47 (2009), pp. 2708–2734.
[37] L. Rayleigh, *On the dynamical theory of gratings*, Proc. Roy. Soc. London Ser. A, 79 (1907), pp. 399–416.
[38] S. O. Rice, *Reflection of electromagnetic waves from slightly rough surfaces*, Comm. Pure Appl. Math., 4 (1951), pp. 351–378.
[39] V. Rokhlin and M. Tygert, *Fast algorithms for spherical harmonic expansions*, SIAM J. Sci. Comput., 27 (2006), pp. 1903–1928.
[40] R. Sakamoto, *Hyperbolic Boundary Value Problems*, Cambridge University Press, Cambridge, UK, 1982.
[41] J. Shen, *Efficient spectral-Galerkin method* I. *Direct solvers for second- and fourth-order equations using Legendre polynomials*, SIAM J. Sci. Comput., 15 (1994), pp. 1489–1505.
[42] J. Shen, T. Tang, and L. L. Wang, *Spectral Methods: Algorithms, Analysis and Applications*, Springer Ser. Comput. Math. 41, Springer-Verlag, Berlin, Heidelberg, 2011.
[43] K. L. Shlager and J. B. Schneider, *A selective survey of the finite-difference time-domain literature*, IEEE Antennas Propagation Mag., 37 (1995), pp. 39–57.
[44] I. L. Sofronov, *Conditions for complete transparency on a sphere for a three-dimensional wave equation*, Dokl. Akad. Nauk, 326 (1992), pp. 953–957.
[45] I. L. Sofronov, *Artificial boundary conditions of absolute transparency for two- and three-dimensional external time-dependent scattering problems*, European J. Appl. Math., 9 (1998), pp. 561–588.
[46] R. Suda and M. Takami, *A fast spherical harmonics transform algorithm*, Math. Comp., 71 (2001), pp. 703–716.
[47] P. N. Swarztrauber and W. F. Spotz, *Generalized discrete spherical harmonic transforms*, J. Comput. Phys., 159 (2000), pp. 213–230.
[48] G. Szegö, *Orthogonal Polynomials*, 4th ed., Amer. Math. Sci. Collog. Publ. 23, American Mathematical Society, Providence, RI, 1975.
[49] A. Taflove and S. C. Hagness, *Computational Electrodynamics: The Finite-Difference Time-Domain Method*, 3rd ed., Artech House, Boston, MA, 2005.
[50] L. L. Thompson and R. N. Huan, *Computation of far-field solutions based on exact nonreflecting boundary conditions for the time-dependent wave equation*, Comput. Methods Appl. Mech. Engrg., 190 (2000), pp. 1551–1577.
[51] L. Ting and M. J. Miksis, *Exact boundary conditions for scattering problems*, J. Acoust. Soc. Amer., 80 (1986), pp. 1825–1827.
[52] G. N. Watson, *A Treatise of the Theory of Bessel Functions*, 2nd ed., Cambridge University Press, Cambridge, UK, 1966.
[53] W. L. Wood, *Practical Time-Stepping Schemes*, Oxford Appl. Math. Comput. Sci. Ser., Clarendon Press, Oxford University Press, New York, 1990.